



Research paper

Design, synthesis, and *in vitro* biological evaluation of *meta*-sulfonamidobenzamide-based antibacterial LpxH inhibitors

Andrea Benediktsdottir^{a,*}, Sanjeewani Sooriyaarachchi^b, Sha Cao^c, Nina E. Ottosson^{d,e}, Stefan Lindström^a, Bo Lundgren^f, Katharina Kloditz^f, Daina Lola^g, Olga Bobileva^g, Einars Loza^g, Diarmaid Hughes^c, T. Alwyn Jones^b, Sherry L. Mowbray^{b,h}, Edouard Zamaratski^a, Anja Sandström^{a,1}, Anders Karlén^{a,1,*}

^a Department of Medicinal Chemistry, BMC, Uppsala University, Box 574, SE-75123, Uppsala, Sweden

^b Department of Cell and Molecular Biology, BMC, Uppsala University, Box 596, SE-75123, Uppsala, Sweden

^c Department of Medical Biochemistry and Microbiology, BMC, Box 582, SE-75123, Uppsala, Sweden

^d Department of Biomedical and Clinical Sciences, BKV, Linköping University, SE-581 85, Linköping, Sweden

^e Chemical Biology Consortium Sweden (CBCS), Science for Life Laboratory, Tomtebodavägen 23a, 171 65, Solna, Sweden

^f Department of Biochemistry and Biophysics, Stockholm University, Biochemical and Cellular Assay Unit, Drug Discovery and Development Platform, Science for Life Laboratory, Tomtebodavägen 23A, SE-17165, Solna, Sweden

^g Latvian Institute of Organic Synthesis, Riga, LV-1006, Latvia

^h Science for Life Laboratory, Uppsala University, Box 596, SE-751 24, Uppsala, Sweden

ARTICLE INFO

Handling editor: Z Liu

Keywords:

LpxH inhibitors
Lipopolysaccharide synthesis
hERG ion channel affinity
Antimicrobial drug discovery
Gram-negative bacteria
Meta-sulfonamidobenzamide
N-demethylation
Lipid A

ABSTRACT

New antibacterial compounds are urgently needed, especially for infections caused by the top-priority Gram-negative bacteria that are increasingly difficult to treat. Lipid A is a key component of the Gram-negative outer membrane and the LpxH enzyme plays an important role in its biosynthesis, making it a promising antibacterial target. Inspired by previously reported *ortho*-*N*-methyl-sulfonamidobenzamide-based LpxH inhibitors, novel benzamide substitutions were explored in this work to assess their *in vitro* activity. Our findings reveal that maintaining wild-type antibacterial activity necessitates removal of the *N*-methyl group when shifting the *ortho*-*N*-methyl-sulfonamide to the *meta*-position. This discovery led to the synthesis of *meta*-sulfonamidobenzamide analogs with potent antibacterial activity and enzyme inhibition. Moreover, we demonstrate that modifying the benzamide scaffold can alter blocking of the cardiac voltage-gated potassium ion channel hERG. Furthermore, two LpxH-bound X-ray structures show how the enzyme-ligand interactions of the *meta*-sulfonamidobenzamide analogs differ from those of the previously reported *ortho* analogs. Overall, our study has identified *meta*-sulfonamidobenzamide derivatives as promising LpxH inhibitors with the potential for optimization in future antibacterial hit-to-lead programs.

1. Introduction

Antimicrobial resistance (AMR) is spreading faster than new antibiotics are being developed, causing a crisis that threatens modern healthcare systems [1]. In Europe alone, bacterial AMR was associated with 541,000 deaths in 2019, of which over 133,000 were directly attributable to resistant infections [2]. The global burden of AMR is largely driven by six key bacterial pathogens—*Escherichia coli*, *Staphylococcus aureus*, *Klebsiella pneumoniae*, *Pseudomonas aeruginosa*,

Streptococcus pneumoniae, and *Acinetobacter baumannii*—which collectively account for nearly 90 % of AMR-related deaths [3]. The World Health Organization (WHO) in their bacterial priority pathogens list from 2024 highlights the development of new antibiotics targeting Gram-negative bacteria (GNB) as the most critical priority in the fight against AMR. At the top of their list are the three particularly dangerous strains: carbapenem-resistant *Klebsiella pneumoniae* and *Acinetobacter baumannii*, along with third-generation cephalosporin-resistant *Escherichia coli* [4]. These pathogens are considered the highest priority due to

* Corresponding authors.

E-mail addresses: andrea.benediktsdottir@ilk.uu.se (A. Benediktsdottir), anders.karlen@ilk.uu.se (A. Karlén).

¹ Equal contribution.

<https://doi.org/10.1016/j.ejmech.2024.116790>

Received 3 July 2024; Received in revised form 15 August 2024; Accepted 19 August 2024

Available online 22 August 2024

0223-5234/© 2024 The Authors. Published by Elsevier Masson SAS. This is an open access article under the CC BY license (<http://creativecommons.org/licenses/by/4.0/>).

their resistance to multiple drugs and the severe infections they cause.

Despite the urgency, the clinical pipeline intended to generate new drugs remains inadequate. In 2023, out of 57 traditional antibiotic agents undergoing clinical trials, only 32 exhibited activity against one or more of these critical priority pathogens, and many of these targeted mechanisms where resistance is already established [5]. In addition, for candidates targeting GNB, clinical trial failures are frequently due to safety issues, highlighting the complex challenge of balancing efficacy with safety [6]. This underlines the pressing need to identify novel antibiotics that act on new bacterial targets within GNB, ideally without existing resistance, and focusing on minimizing potential toxic effects early in the process.

The complex structure of the GNB cell wall and membranes provides a wealth of potential and currently unexploited targets for inhibition by antibiotics. The outer membrane of GNB is organized as an asymmetric bilayer, with lipopolysaccharides (LPS) in the outer leaflet and phospholipids in the inner leaflet. This arrangement establishes a complex permeability barrier allowing for selective permeation of nutrients but forming a robust barrier against many other external molecules, including antibiotics. LPS are anchored to the outer membrane by lipid A, a glucosamine-based lipid that is concentrated in the outer leaflet and found in most GNB. Alongside the elucidation of the lipid A structure [7], lipid X was discovered as a precursor [8]. The chemical characterization of lipid X as 2,3-di-acylglucosamine 1-phosphate, and further studies, facilitated Raetz and colleagues in describing the “Raetz pathway” for lipid A biosynthesis [9–12]. The nine enzymes of this pathway in *E. coli* act in the order LpxA, LpxC, LpxD, LpxH, LpxB, LpxK, KdtA, LpxL, and LpxM; they are structurally and functionally conserved between GNB species [12]. In the fourth step of the Raetz pathway, the pyrophosphate moiety of UDP-2,3-diacylglucosamine is hydrolyzed to yield uridine monophosphate (UMP) and lipid X. This step is catalyzed by LpxH in ~70 % of GNB, including the WHO critical priority pathogens *E. coli*, *K. pneumoniae*, and *A. baumannii*, and by LpxI in the remaining 30 % (except for LpxG found in *Chlamydia trachomatis*) [13–15]. Inhibiting LpxH disrupts the biosynthesis of lipid A and causes the accumulation of pathway intermediates in the inner membrane, leading to a toxic state, ultimately resulting in cell death [16,17]. LpxH is a peripheral membrane protein located in the cytosol. Its structure was solved first in 2016 from *Haemophilus influenzae* [18] and shortly after from *P. aeruginosa* [13], revealing a catalytic domain with homology to metallophosphoesterases containing a dimanganese-cluster, with a helical lid domain inserted. The absence of a mammalian homologue for LpxH underscores its potential as an excellent antibiotic target.

In 2015, the first LpxH inhibitor, a sulfonyl piperazine referred to as AZ1 (Fig. 1a), was discovered by a high-throughput phenotypic screen. This compound exhibited no antibacterial activity against wild-type *E. coli* but did have potent activity on an efflux-defective *E. coli* strain (MIC = 0.25 µg/mL) [19], which led to subsequent studies of a series of sulfonyl piperazine analogs with modest improvements over AZ1 [20–22]. Efforts have been invested in designing compounds that reach and capture the manganese cluster in the active site, having a hydroxamate tail on the right-hand side (i.e. JH-LPH-50 (Fig. 1b)). Despite a significant improvement of enzyme inhibition, the antibacterial activity of these analogs on wild-type *K. pneumoniae* was significantly reduced compared to the non-chelating analog [23]. Researchers from the EU’s Innovative Medicines Initiative program called ENABLE reported the discovery of LpxH inhibitors with an optimized right- and left-hand side of the sulfonyl piperazine scaffold (Fig. 1c), resulting in LpxH inhibitors with potent wild-type activity on both *E. coli* and *K. pneumoniae* isolates (MIC = 0.5–2 µg/mL). This new class of LpxH inhibitors, *ortho*-*N*-methyl-sulfonamidobenzamide-based sulfonyl piperazine analogs (EBL-analogs), was patented in 2022 [24]. Further optimization of the EBL-analogs (Fig. 1c), addressing issues such as high protein binding, poor solubility, and low metabolic stability resulted in excellent *in vivo* activity against murine-bloodstream infections caused by *E. coli* and *K. pneumoniae* [25]. In 2023, Roche patented highly active sulfonyl

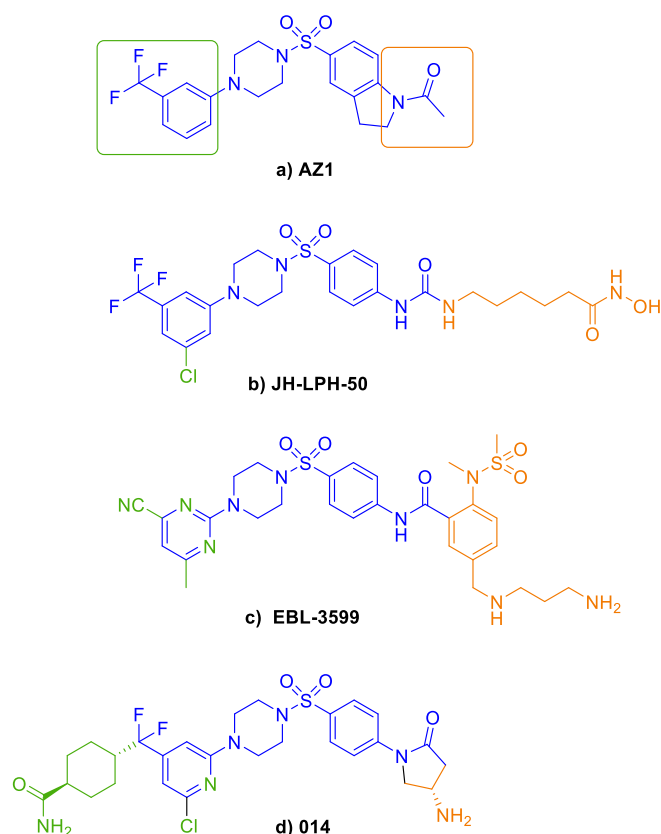


Fig. 1. Selected examples of reported LpxH inhibitors highlighting the optimization strategies of the sulfonyl-piperazine scaffold (blue), right-hand side modification (orange), and left-hand side modification (green). **a)** The first reported LpxH inhibitor, AZ1 [19]. **b)** an extended *N*-acyl chain analog JH-LPH-50 [23]. **c)** Optimized sulfonyl piperazine EBL-inhibitors from the WO2022220725 patent [24]. **d)** Optimized sulfonyl piperazine LpxH inhibitors from Roche R&D WO2023061617 patent [26].

piperazinyl-based compounds that target LpxH with *E. coli* wild-type activity (MIC) as potent as 0.3 µg/mL [26]. The optimization involved incorporating an amino pyrrolidinone on the right-hand side and introducing more polar tails with increased *sp*³-fraction on the left-hand side (Fig. 1d).

The high failure rate of promising candidates in antibiotic development pipelines highlights the need for developing multiple series of close analogs to prototype compounds [27]. New generations can then rapidly be brought into play if undesirable findings terminate the prototype candidate, and they can also be used to expand knowledge of structure-activity/toxicity relationships associated with the scaffold. Thus, the purpose of the current study was to explore an altered substitution pattern of the right-side benzamide motif of the recently reported *ortho*-*N*-methyl-sulfonamidobenzamide-based EBL-analogs.

Here we report the design, synthesis, and *in vitro* biological evaluation of *meta*-sulfonamidobenzamide derivatives together with the crystal structure of one of them in complex with LpxH. In addition, the crystal structure of one of the *ortho*-sulfonamidobenzamide analogs was determined. The inhibition of LpxH enzyme activity and antibacterial activity against a panel of GNB strains are presented, as well as an evaluation of their effects on hemolysis, cytotoxicity, and on the potassium ion channel (hERG), inhibition of which is associated with increased risk of cardiotoxicity. The results are compared with those for the *ortho*-substituted sulfonamide analogs.

2. Results and discussion

2.1. Meta-sulfonamide hit identification

Comparing the antibacterial properties of AZ1 with the newly developed LpxH inhibitors (Fig. 1) showed that the structural motif on the right-hand side has a decisive effect on the antibacterial profile. The LpxH inhibitors previously developed in our lab all contain an *N*-methylated sulfonamide in the *ortho*-position on ring 4 as in **S1** seen in Fig. 2a. In this work, we wanted to see what changes in the ring 4 region are allowed that could give rise to new series of inhibitors. This led to the design of analog **S3** (Fig. 2b), where the *N*-methylated sulfonamide was moved to the *meta*-position on ring 4. This shift resulted in an analog that was inactive on wild-type *E. coli* but had activity on the efflux-deficient strain (ΔtolC MIC <0.125 $\mu\text{g/mL}$). Interestingly, when we removed the methyl group from the sulfonamide nitrogen, resulting in analog **S4** (Fig. 2b), the compound was again active on wild-type *E. coli* (MIC = 4 $\mu\text{g/mL}$). In contrast, the desmethylated *ortho*-substituted analog **S2** was inactive. **S3** and **S4** are equally active on the ΔtolC efflux-deficient strain (MIC = 0.125 $\mu\text{g/mL}$), indicating that the *N*-methyl group modulates the susceptibility of the *meta*-compounds to efflux. Predicting the impact of small structural substitutions on efflux pump susceptibility is challenging. However, recent studies have showed that small structural modifications can convert an efflux substrate into an efflux evader [28–31]. These findings led us to synthesize a series of analogs with the free sulfonamide in the *meta*-position. The initial analogs **S1–S4** contained dichlorobenzene as ring 1, which was replaced with the more polar pyrimidine ring previously shown to be beneficial for solubility of the *ortho*-*N*-methyl-sulfonamidobenzamide-based EBL-analogs [25].

2.2. X-ray crystallography and design

We have solved two LpxH-inhibitor complexes to aid in the optimization of the *meta*-series. The *K. pneumoniae* enzyme (*KpLpxH*) was solved in complex with the *meta*-sulfonamide-substituted analog **S4** at 2.2 Å resolution (PDB entry code 9ENG), and the *E. coli* enzyme (*EcLpxH*) in complex with the equivalent *ortho*-*N*-methylated sulfonamide analog **S1** at 1.6 Å resolution (PDB entry code 8S7F). Each inhibitor binds in the substrate-binding site of the respective enzyme, making essentially identical sets of enzyme-inhibitor interactions. Thus, an alignment of the enzyme structures results in closely superimposed inhibitors with clear distinction between the placements of the *ortho*- and *meta*-substitutions (Fig. 2c). As seen in previous complexes reported by Huseby et al. [25] with *ortho*-substituted compounds, both **S1** and the *meta*-substituted analog **S4** adopt an L-shape, with a central core

superimposable with the conserved scaffold (rings 2 and 3). In all cases, one oxygen of the central sulfonamide moiety makes a hydrogen bond with the main-chain nitrogen of Trp46, and a close contact with the main-chain oxygen of Arg80. As for the *ortho*-complexes, the guanidino group of Arg80 stacks on one face of ring 3 in the *meta*-complex, making a cation- π -interaction (Fig. 3); the arginine's side-chain conformation is different from that seen in the complex with the reaction product, lipid X (Fig. 4). For both the *ortho*- and *meta*-complex, one face of ring 4 makes edge-face interactions with Phe128, and the carbonyl oxygen of the amide linking rings 3 and 4 makes a hydrogen bond to the side-chain nitrogen of Asn79. The *ortho*-substituted benzamide (ring 4) points toward the catalytic site, positioned so that one oxygen atom of the sulfonamide makes a hydrogen bond with the side chain of Arg80 [25]. However, with the sulfonamide in a *meta*-position, the interaction with Arg80 is lost, exchanged for van der Waals interactions of its methyl group with the ring of Tyr125 (Fig. 3). It was observed that the hydroxymethyl group on the glucosamine of lipid X in the previously-published structure of *EcLpxH* in complex with lipid X (PDB: 8QJZ) [25] makes a hydrogen bond with a side-chain nitrogen of His195 (O–N distance 2.6 Å) and the tetrahydropyranol proton of lipid X makes a hydrogen bond with a side-chain nitrogen of Lys167 (O–N distance 2.7 Å) (Fig. 4). We envision that new compounds could be designed to make better use of the possible interactions in this region. However, in this work the focus was to introduce ring 4 extensions onto the *meta*-scaffold similar to those on the *ortho*-scaffold to assess the compatibility of similar strategies with the *meta*-core. These extensions are cationic amines that are commonly known to be able to improve compound accumulation in GNB [32]. We also wanted to explore whether replacing the benzene ring 4 with pyridine would have an effect on enzyme affinity or biological activity, as it has recently been linked with less efflux in GNB when introduced in antibacterial compounds [29].

Accordingly, we prepared seven new LpxH inhibitors (**4a**, **4c**, **6a-d** and **7**) with the polar pyrimidine as ring 1 and the *meta*-sulfonamide on ring 4, and with pyridine (**4c** and **7**) and phenyl (**4a** and **6a-d**) as ring 4, including cationic amines as substituents, seen in Schemes 2 and 3.

2.3. Synthesis

The *meta*-sulfonamide benzoic acids **2a-b** were made by sulfonylation of aniline **1a-b** (Scheme 1). Due to poor nucleophilicity of the 2-aminopyridine [33], following the same sulfonylation procedure for the pyridine analog **2c** was not feasible (yields <10 %). Therefore, the *meta*-sulfonamide pyridine building block **2c** was prepared via Buchwald-Hartwig C–N cross-coupling starting with a dichloro-pyridine **1c** (Scheme 1). The **1a-c** esters were then hydrolyzed to give the corresponding benzoic acids **2a-c**.

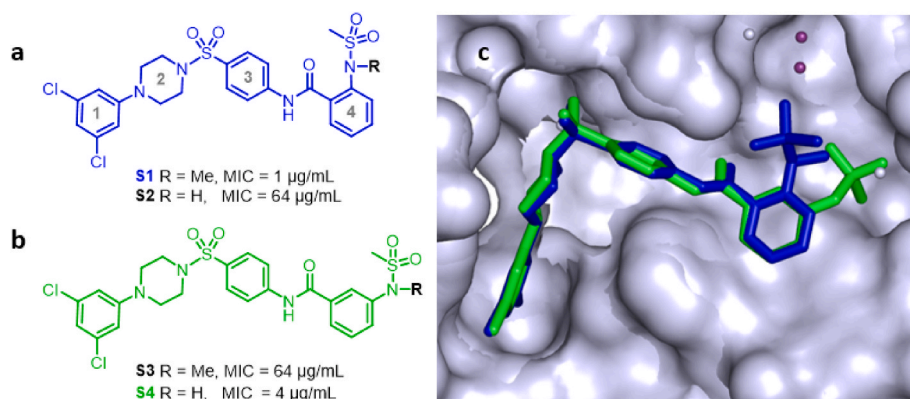


Fig. 2. a) Chemical structures of the *ortho*-sulfonamidobenzamide-based LpxH inhibitors **S1** and **S2** and their antibacterial activity (MIC) on wild-type *E. coli*. b) Chemical structures of the *meta*-sulfonamidobenzamide LpxH inhibitors **S3** and **S4** and their antibacterial activity (MIC) on wild-type *E. coli*. c) Surface representation of LpxH X-ray structure with **S1** (blue) in complex with *EcLpxH* (1.6 Å, PDB: 8S7F) and **S4** (green) overlaid in complex with *KpLpxH* (2.2 Å, PDB: 9ENG) shown in stick representation. The Mn^{2+} ions are shown as purple spheres and waters as grey spheres.

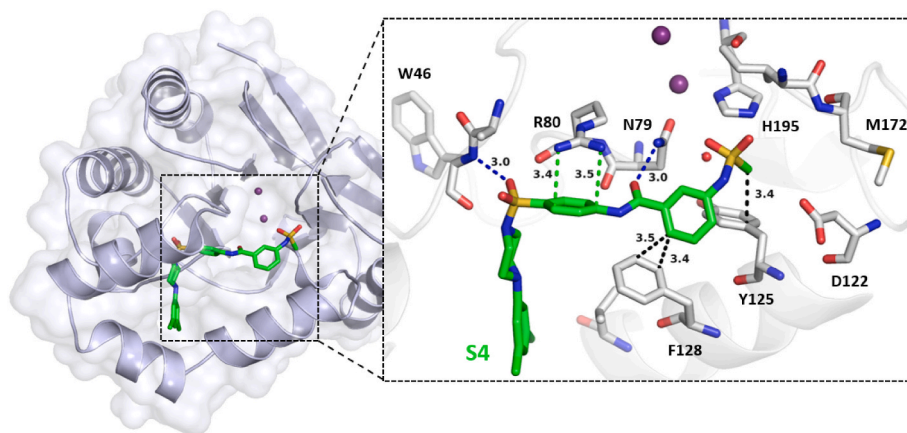


Fig. 3. Detailed interactions in the active site of LpxH with S4. Compound S4's interactions with *KpLpxH*, the Mn^{2+} ions are shown as purple spheres. Hydrogen bonds are shown with blue dashed lines, cation- π interactions are shown in green, edge-to-face interaction and hydrophobic van der Waals interaction are shown in black. (*KpLpxH* 2.2 Å, PDB: 9ENG).

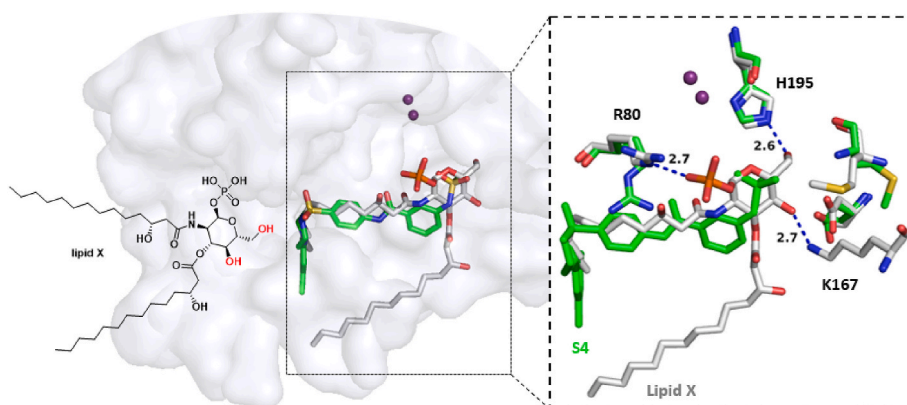
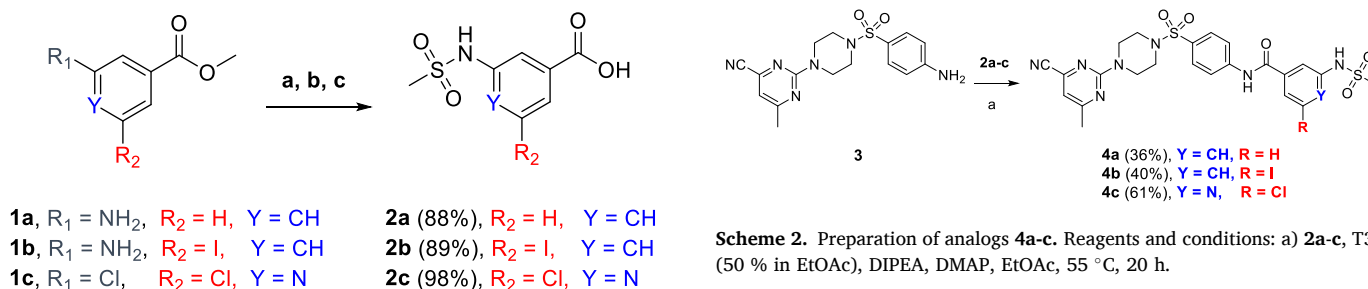


Fig. 4. Lipid X in complex with *EclpxH* (grey sticks) (PDB: 8QJZ) and its interactions with the protein. Also shown is S4 (PDB: 9ENG, in green sticks) superimposed on *EclpxH*. The Mn^{2+} ions are shown as purple spheres.



Scheme 1. Preparation of meta-sulfonamide building blocks **2a-c**. Reagents and conditions: a) for **2a-b**; $MeSO_2Cl$, Et_3N , DCM, 0 °C, 2 h. b) for **2c**; methanesulfonamide, K_3PO_4 , Xantphos and Pd_2dba_3 in toluene, 120 °C, 50 min. c) $LiOH$, THF/EtOH/ H_2O (3:2:1), overnight at r.t.

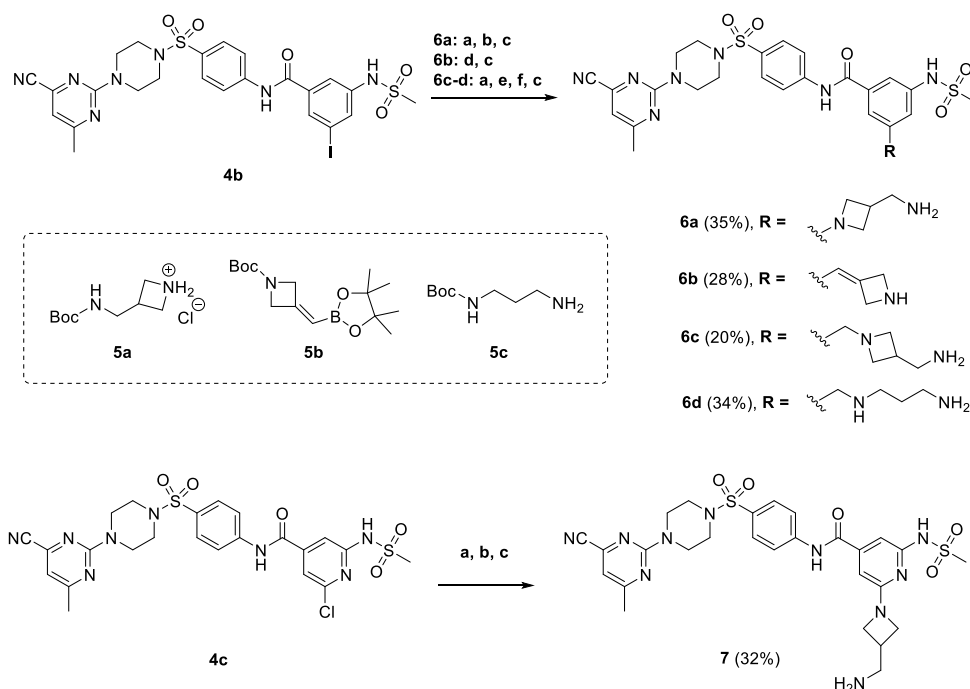
The benzoic acids **2a-c** were coupled to aniline **3** [24] with propylphosphonic anhydride (T3P) coupling, resulting in the amides **4a-c** (Scheme 2). Compound **4a** was prepared to enable a direct comparison to the *ortho*-analog **EBL-3339** (Scheme 3B). The iodo-intermediate **4b** was used to make the final compounds **6a-d** via different synthetic routes seen in Scheme 3A. For preparation of **6a**, the sulfonamide was first protected with chloromethyl ethyl ether (EOM-Cl) for better yields in Buchwald-Hartwig amination of Boc-azetidone **5a**, followed by TFA removal of the Boc group (Scheme 3A). Compound **6b** was prepared in

Scheme 2. Preparation of analogs **4a-c**. Reagents and conditions: a) **2a-c**, T3P (50 % in EtOAc), DIPEA, DMAP, EtOAc, 55 °C, 20 h.

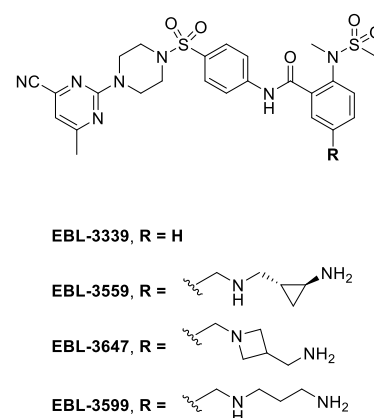
two steps via Suzuki-Miyaura cross-coupling of the Boc-azetidone boronic acid **5b** to the iodo-intermediate **4b** followed by TFA deprotection of Boc. Compounds **6c-d** were prepared in four steps; first the sulfonamide was protected with EOM-Cl, followed by carbonylation transformation of the iodo-benzamide **4b** with formic acid to form an aldehyde intermediate that underwent reductive amination with the commercially available amines **5a** or **5c** to form the benzylic amines, and finally TFA deprotection of the Boc-group (Scheme 3A). The chloro-intermediate **4c** was used to make the final pyridine-based compound **7** via same synthetic routes by which compound **6a** was made.

For comparison, we included the structures and *in vitro* biological data of four previously prepared LpxH inhibitors: **EBL-3339**, **EBL-3559**, **EBL-3647**, **EBL-3599** (Scheme 3B), the latter two being the most active LpxH inhibitors described and evaluated *in vivo* by Huseby et al. [25].

A. Synthesis of the meta-series



B. For comparison: corresponding ortho-analogs previously reported



Scheme 3. A. Preparation of analogs **6a-d** and **7**. Reagents and conditions: a) EOM-Cl, DIPEA, r.t., 20 h. b) **5a**, toluene, XantPhos or RuPhos, Pd(dba)₃, K₃PO₄ or Cs₂CO₃, 90 °C, overnight. c) TFA/DCM (1:1), r.t. d) **5b**, Pd(PPh₃)₄, K₂CO₃, toluene/EtOH (1:1), 4 h, 85 °C. e) Iodine, Ph₃P, toluene, r.t., 30 min; then **4b**, Pd(OAc)₂, Et₃N, formic acid, 80 °C, 1 h. f) **5a** or **5c**, THF/MeOH (1:1), r.t., 20h.; then NaBH(OAc)₃, MgSO₄, 3 h. B. Structures of corresponding *ortho*-analogs from the EBL-series reported in WO2022220725 patent and Huseby et al. [24,25].

2.4. In vitro biology

2.4.1. Biochemistry and microbiology

Compounds **4a**, **4c**, **6a-d**, and **7** were evaluated in a colorimetric coupled enzymatic assay similar to that developed by Lee et al. [21] where the released inorganic phosphate is quantified with malachite green. Here we report the data (Table 1) as percentage inhibition of the activity of LpxH. The compounds prepared in this work inhibited LpxH activity by 54–92 % at 100 nM inhibitor concentration, which ranks them as almost equipotent to the *ortho*-analogs. These results show that

extensions towards the solvent on the *meta*-substituted compounds did not disrupt binding affinity to LpxH. The compounds were also evaluated for their minimal inhibitory concentration (MIC), against wild-type *E. coli*, an efflux pump-deficient *E. coli* (Δ tolC) strain, and wild-type *K. pneumoniae*. All compounds show potent antibacterial activity on the efflux pump-deficient *E. coli* strain with MIC <0.5 μ g/mL. However, when the cationic amine extensions are introduced on the *meta*-core, there is a slight reduction in antibacterial activity on *E. coli* Δ tolC (Table 1). Extensions on the aromatic ring 4 revealed that the benzylic amines **6c-d** outperformed (wild-type *E. coli* MIC = 4 μ g/mL) the more

Table 1

In vitro biology results for the *meta*-substituted compounds (**4a-7**) compared to previously reported *ortho*-substituted LpxH inhibitors (EBL-series).

ring 4 substitution	Cpd no.	EcLpxH Enzyme	<i>E. coli</i>		<i>K. pneumoniae</i>	Hemolysis	Cytotoxicity	hERG % inhibition ^d	
			% inhibition at 100 nM	WT ^a (μ g/mL)	Δ tolC ^b (μ g/mL)	WT ^c (μ g/mL)	%	IC ₅₀ (μ M)	10 μ M
<i>meta</i> -NHSO ₂ Me	4a	75	4	0.125	2	0.05 ± 0.01	–	3 ± 1	12 ± 1
	4c	54	8	≤ 0.125	4	0.02 ± 0.01	>50	2 ± 3	0 ± 3
	6a	92	64	0.25	32	0.12 ± 0.02	>100	5 ± 4	9 ± 4
	6b	86	64	0.5	16	0.17 ± 0.04	>100	4 ± 2	24 ± 2
	6c	89	16	0.25	4	0.06 ± 0.01	–	4 ± 1	7 ± 3
	6d	63	8	0.5	4	0.08 ± 0.04	>100	3 ± 1	9 ± 1
	7	80	8	0.5	4	0.12 ± 0.04	>100	1 ± 1	0 ± 1
<i>orto</i> -NMeSO ₂ Me	EBL-3339 ^e	100	2	≤ 0.125	2.0	0.05 ± 0.02	29	14 ± 2	24 ± 2
	EBL-3559 ^e	100	2	≤ 0.125	0.5	0.35 ± 0.05	47	9 ± 4	28 ± 8
	EBL-3647 ^e	71	2	≤ 0.125	0.5	0.13 ± 0.19	54	5 ± 1	16 ± 2
	EBL-3599 ^e	69	2	≤ 0.125	1.0	0.06 ± 0.01	55	4 ± 2	11 ± 2

^a *E. coli* ATCC 25922 WT.

^b *E. coli* Δ tolC (CH3130, efflux-defective mutant isogenic to ATCC 25922).

^c *K. pneumoniae* ATCC 13883 WT.

^d Inhibition of hERG (hKv11.1) ion current in CHO-KV11.1 cells on the automated patch-clamp system QPatch II 48.

^e Compounds for comparison, reported in Huseby et al. and WO2022220725 patent [24,25].

rigid extensions **6a-b** that were inactive due to efflux. An interesting effect observed when introducing nitrogen in the aromatic ring is that the wild-type inactive **6a** becomes relatively active (**7**, MIC = 8 µg/mL). All compounds show good antibacterial activity on wild-type *K. pneumoniae* (MIC = 2–4 µg/mL) except for **6a-6b** (MIC = 16–32 µg/mL). A similar trend was also seen for **6a-b** on wild-type *E. coli* (MIC = 64 µg/mL).

2.4.2. Inhibition of hERG K⁺ channel and toxicity

As seen in Table 1, the final compounds did not display any hemolytic effects on red blood cells (0.02–0.17 %) similarly to the corresponding EBL-compounds, where values below 1 % are considered acceptable. None of the *meta*-sulfonamidobenzamides caused cytotoxic effects (IC₅₀: >100 µM) whereas the *ortho*-*N*-methyl-sulfonamidobenzamide analogs showed relatively higher cytotoxicity, where **EBL-3339** was the most toxic, inhibiting HepG2 with an IC₅₀ of 29 µM.

Blockade of the voltage-gated potassium channel Kv11.1, hereinafter referred to as hERG (encoded by the human ether-a-go-go-related gene (hERG) KCNH2 [34]), is considered a significant hurdle during lead optimization, as it may suggest problems with possible induced “torsade de pointes” arrhythmias and sudden cardiac death [35]. Therefore, in this work, we evaluated both the original *ortho*- and the newly prepared *meta*-series for such off-target effects. The electrophysiology recording of the hERG channel current was carried out on epithelial CHO cells with 10 and 30 µM concentrations of the compounds. The hERG-blocking effect of the compounds is listed in Table 1, as a percentual inhibitory effect. At 10 µM concentration, most of the inhibitors show less than 10 % inhibition of the hERG ion channel, except for the *ortho*-analog **EBL-3339** with 14 % inhibition. At the higher concentration (30 µM), the *meta*-inhibitors show little effect (0–12 %), except for **6b** with 24 % inhibition. The *ortho*-inhibitors caused 11–28 % inhibition of the ion channel, with **EBL-3559** showing the highest inhibition (Table 1).

It is noteworthy that most of the compounds contain cationic amines attached to the hydrophobic aromatic core, commonly known as a risk for hERG blockade [36,37]. However, our findings demonstrate that on this scaffold, the presence of cationic amines does not correlate with increased hERG inhibition. Instead, our work shows that the hERG inhibition can be modulated by a change of substitution pattern on ring 4.

3. Conclusions

To date, there is no antibiotic available in the clinic targeting the LpxH enzyme. Nonetheless, LpxH is considered a highly interesting antibiotic target. Promising *ortho-N*-methyl-sulfonamidobenzamide based LpxH inhibitors were recently discovered in our lab. In the current study, we wanted to explore what changes in the benzamide ring are allowed that could give rise to a new series of inhibitors. We identified *meta*-sulfonamidobenzamide derivatives as new hits, solved a co-crystal structure with the enzyme, and prepared substituted derivatives (**4a**, **4c**, **6a-d**, and **7**) targeting LpxH. The compounds were assessed for their inhibition of LpxH activity, antibacterial activity, and toxic effects. The compounds effectively inhibited LpxH, being almost equipotent to the *ortho*-analogs. Antibacterial evaluations showed high potency against efflux pump-deficient *E. coli*. When adding extensions to the aromatic ring 4 benzylic amines outperformed the more rigid extensions with regards to wild-type antibacterial activity, apparently because the rigid analogs were rapidly pumped out by efflux pumps. Most compounds demonstrated potent antibacterial activity against wild-type *K. pneumoniae*. Importantly, our findings demonstrate that desmethylation and changing the substitution pattern on the benzamide to the *meta*-position resulted in reduced cytotoxicity compared to the *ortho*-series. Neither the *meta*-analogs nor the *ortho*-analogs caused hemolysis and both showed little to no hERG ion channel inhibition, although the *meta*-sulfonamidobenzamide displayed a moderately enhanced safety profile, particularly at higher concentrations. These findings provide

important insights into the antibacterial efficacy and safety profile of the sulfonamidobenzamide derivatives, as well as identifying the *meta*-analogs as a promising LpxH inhibitors, guiding future optimization for potential therapeutic applications.

4. Experimental section

4.1. Antibacterial activity

For the minimal inhibitory concentration (MIC) assay, the compounds were prepared in Mueller-Hinton II medium and dispensed into a 96-well round-bottomed plate to give final assay concentrations from 64 mg/mL down to 0.25 mg/mL (two-fold dilution series in 10 wells, with two control wells: medium control with no bacteria or compound, and growth control with bacteria added but no compound). Plates were covered and incubated without shaking for 16–20 h at 35 °C ± 2 °C. MIC was read visually, as complete inhibition of growth by the unaided eye, using the medium-only wells as the control [38].

4.2. In vitro cytotoxicity and hemolysis

Fluorometric microculture cytotoxicity assay (FMCA) [39]. The cell line HepG2 was obtained from ATCC, and cultured in Dulbecco's Modified Eagle Medium (DMEM, Sigma, #11995-065) supplemented with 10 % fetal bovine serum (Sigma, #F9665), and penicillin/streptomycin (100 U/100 µg/mL, Sigma P4333). HepG2 cells were passaged 2 times/week and used maximally for 20 passages. The cells were tested to be mycoplasma free. Procedure: The FMCA is based on measurement of fluorescence generated from hydrolysis of fluorescein diacetate (FDA) to fluorescein by cells with intact plasma membranes. HepG2 cells (4000/well) were seeded in 384-well cell culture microplates (Corning #3746 or Greiner #781090) using the Thermo Multidrop 384 (Labsystems) and cultured overnight before inhibitors were added. The required amounts of compounds were transferred to a microplate (384-Well PP 2.0 Microplate, Labcyte, #PP-0200) using the Echo 550 acoustic liquid handler and then resuspended in 20 µL DMEM medium. The plate was placed on a shaker (MixMate, Eppendorf) for 1 h at 1200 rpm and centrifuged (Hermle Z446, 200×g, 1 min) before the compounds were added to the cells using the Janus liquid handler (PerkinElmer). Each compound was dispensed for dose-response, with nine two-fold dilutions in duplicate with the highest concentration of 100 µM, to generate IC₅₀s. Bortezomib (2 µM) was used as positive control, and dose response testing of doxorubicin (highest concentration 10 µM) was performed repeatedly to follow assay performance over time. After 72 h exposure of the cells to the drugs in an incubator (at 37 °C, humidity 95 %, 5 % CO₂) the 384-well plates were centrifuged (200×g, 60 s), the culture medium was removed by a Biotech ELx405 Select CW washer (Biotek, Winooski, VT, USA) and 70 µL phosphate buffered saline (PBS, Sigma) was added to the wells. The plates were then centrifuged (200×g, 60 s, Hermle Z446) and the PBS was removed by the Biotech ELx405 Select CW washer after which 50 µL/well of assay buffer (HEPES-buffered saline containing 0.02 M HEPES, 150 Mm NaCl, 0.5 mM MgCl₂ and 0.5 mM CaCl₂ and 0.5 µg/ml FDA, pH 7.4) was added to the plates using a Multidrop 384 (Thermo Fischer Scientific, NY, USA). The plates were then incubated for 50 min in the incubator (37 °C, humidity 95 %, 5 % CO₂, Thermo Fischer Scientific) before being analyzed in an EnVision 2104 Multilabel Plate Reader (PerkinElmer) with wavelengths set at 475 nm (excitation) and 520 nm (emission). Cytotoxicity was assessed after 72 h with cell survival presented as survival index (SI, percent of control %) defined as fluorescence in test wells in percent of control cultures with blank values subtracted. Criteria for a successful assay included a signal-to-noise ratio in control cultures >10, CV < 30 % and a positive control (Bortezomib) SI of <5 %. The half maximal inhibitory concentration (IC₅₀) was determined from log concentration-effect curves in CDD using a non-linear regression analysis. The final compounds were evaluated for hemolytic effects using red

blood cells from heparinized human blood according to the previously described protocol [38].

4.3. Inhibition evaluation on hERG K^+ ion channel

Automated patch clamp recordings were done at 22 °C on a QPatch II 48 platform (Sophion Bioscience A/S, Copenhagen, Denmark). Freshly harvested cell suspensions (2–3 million cells/ml) were prepared for the experiment by the QPatch II 48 automated cell preparation unit. Cells were centrifuged twice at 150 s at 150 g and washed with an extracellular solution. Cells were handled by the integrated pipetting robot and added to the 48 experiment sites on the planar patch-clamp consumable QPlate. Each experiment site contained an individual pair of recording electrodes and a silicon/glass biochip embedded in the flow channels. Recordings were population patch (10 cells). Once the cells were applied, they were positioned and sealed to the patch holes by a mild suction protocol. Whole-cell access was obtained by another, stronger suction pulse to the cells. The stably expressing cell line CHO-KV11.1 Duo (B'SYS, Witterswil, Switzerland) was used to study the cells' currents on the automated patch-clamp system QPatch II 48. Cell culture and passaging were performed in accordance with the standard operating procedures. The ion channel was expressed constitutively. The cells were harvested in a serum-free medium with Detachin™ (Gentantis, CA, USA) immediately prior to experiment execution. The following extracellular solution (in mM) was used: 145 NaCl; 10 glucose; 4 KCl; 2 CaCl₂; 1 MgCl₂ and 10 HEPES. The osmolarity was 305–308 mOsm and the pH was adjusted to 7.4 with NaOH. The intracellular solution was (in mM): 100 KCl; 4.30 CaCl₂; 4 Mg-ATP; 1.4 MgCl₂; 25/10 KOH/EGTA; 24 KF; and 10 HEPES. The osmolarity was 290–298 mOsm and the pH was adjusted to 7.2 with KOH. Square voltage pulses were run for I(V) relationships using the multi-hole QPlates. Each I(V) step protocol was first run twice in a vehicle (extracellular solution supplemented with 0.43 % DMSO), which served as a current baseline, and then in each of 2 cumulatively rising compound concentrations, followed by a vehicle for recovery. As a control of the assay, a set of vehicles instead of a compound was included in each run. Each solution was added twice (5s between applications: 10 µL per application), and the solution was present for 30 s until the start of electrophysiological recordings. All added solutions contained the same concentration of DMSO (0.43 %). hKV11.1 cells were kept at a holding voltage of –80 mV and briefly hyperpolarized to –100 mV for 100 ms before a 20 ms pulse to –50 mV (for calculations of ohmic leakage). Square voltage pulses were then applied sequentially in 10 mV increments starting from –80 mV, stepping up to 50 mV for 5 s before holding the cell at –50 mV for 2 s (tail current recordings) and stepping back to the holding voltage. The voltage protocol was executed every 150 s.

The data were analyzed using Sophion Analyzer 6.6. The ohmic leakage was subtracted from the tail current. The tail current was measured as the peak value during the first 90 ms of the second –50 mV step, which then was plotted directly against the preceding test voltage to get the G(V) curve. Mean values of were expressed as mean ± SEM (performed in triplicate). For comparisons, a two-way ANOVA test (Gaussian distribution of residuals and equal SDs assumed) with Dunnett's multiple comparisons test was used. GraphPad Prism 8.4.3 was used for statistical analysis.

4.4. Protein production and LpxH inhibition

Cloning, expression and purification of EclpxH and KplpxH were carried out as described previously [25]. For establishing enzymatic inhibition, the AaLpxE-coupled LpxH activity assay was based on a previously published protocol [21], with modifications as described in Huseby et al. [25]. The substrate UDP-DAGn concentration was calculated using a molecular weight of 1016 g/mol, and assuming that all absorbance at 262 nm is due to the UDP moiety, with an extinction coefficient of 9.9 mM⁻¹cm⁻¹. Briefly, the substrate mixture and the

enzyme mixture were prepared, each containing assay buffer (20 mM Tris-HCl at pH 8.0, 0.5 mg/ml BSA, 0.02 % Triton X-100, 1 mM MnCl₂, 1 mM DTT, and 10 % DMSO), and either 40 µM UDP-DAGn or 5 ng/ml LpxH (resulting in final concentrations of 20 µM and 0.1 nM, respectively, in the assay). The inhibitor was added to the enzyme mixture at the desired concentration. The two mixtures were pre-incubated at 37 °C for 10 min before starting the reaction by combining an equal amount of each mixture at 37 °C. Aliquots of 20 µl reaction mixture were removed at 30 min, and added to separate wells in a 96-well half-area plate containing 5 mM EDTA (final concentration) to quench the reaction after 30 min. MBP-AaLpxE was then added to a final concentration of 5 µg/ml in each well, and the samples were incubated for 30 min at 37 °C. The LpxE reaction was then quenched by the addition of 3.75 M formic acid (final concentration) to the reaction mixture. In the following step, malachite green reagent (Sigma Aldrich) was added to a five-fold dilution, and the absorbance at 620 nm was measured using a plate reader (Envision, PerkinElmer) after incubation at room temperature for 30 min. The amount of free inorganic phosphate liberated during the LpxE reaction was calculated from a phosphate standard curve and used to determine the activity of the LpxH enzyme. The standard curve was prepared using the phosphate standard provided with the kit, which is diluted into the reaction buffer to provide a range of phosphate concentrations up to 40 µM (the linear range extends to 200 µM). The assays were run in triplicate.

4.5. Structural biology

For co-crystallization of EclpxH and KplpxH, the inhibitors were added to diluted protein sample (protein:compound ratio 1:10) in the presence of 1 mM MnCl₂; the solution was then concentrated to ~15 mg/mL in 20 mM Tris-HCl, pH 8.0, 300 mM NaCl, 5 % glycerol, 2 mM DTT, and 1 mM MnCl₂, before crystallization screening. The experiments were set up in 2-well MRC plates with a Mosquito crystallization robot (TTP Labtech). Drops consisting of 100 nL protein and 100 nL screening solution were equilibrated against 50 µL of the respective screening solution. Two screens were tested at ambient temperature; crystals appeared overnight in Morpheus III. Crystals were harvested from the wells and cryo-cooled in the respective mother liquor. X-ray data were collected at 100 K at Diamond Light Source (UK), processed with XDS [40], and scaled with AIMLESS [41]. Both complexes suffered from anisotropy in their diffraction. Statistics for X-ray data collection and model refinement are given in [Supplementary Table 1](#). The structures were solved based on molecular replacement using earlier structures [25]. Each model was improved by multiple cycles of restrained crystallographic refinement using REFMAC5 [42] and rebuilt as needed in O [43]. The occupancy of the carbonyl oxygens of residues 213–215 was set to zero at the start of each refinement, and solvents were added using the Water-tools in O, guided by the height of the peaks in the difference Fourier at the three carbonyl oxygens. Initial inhibitor models were built and their stereochemical restraints were generated in O with the Qds-tools. The fit of the inhibitor to the final electron density is good in each complex (see Supplementary Information, [Fig. S1](#)). The overall fit of the main chain of each respective enzyme model is also excellent, with no significant breaks at the RMS of the map, except for one region that is disordered in all enzyme-inhibitor complexes, but well defined in the enzyme-product complex, as described in Huseby et al. [25]. Briefly, the EclpxH/S1 complex was solved at 1.6 Å resolution, and refined to a crystallographic R-factor of 18.4 %, and the KplpxH/S4 complex was solved at 2.2 Å resolution with a crystallographic R-factor of 23.7 %. The lower resolution of the KplpxH/S4 complex and the overall high temperature factor of the model means that the electron density for the *meta*-substitution on ring 4 is well defined but smooth, with the oxygen atoms and methyl group close to the envelope of the density at the RMS of the map. Since we cannot differentiate between oxygen atoms and the methyl group at the resolution of these studies, they have been modelled according to the local set of interactions.

4.6. Chemical synthesis

All reagents and solvents were purchased from Sigma Aldrich, Fisher Scientific, FluoroChem, Enamine and Chemtronica and were used without further purification. Analytical thin layer chromatography (TLC) was performed using Merck aluminum sheets precoated with silica gel 60 F₂₅₄. Column chromatography was performed on Merck silica gel 60 (40–63 μm) ¹H and ¹³C NMR spectra were recorded on Varian and Bruker instruments; ¹H at 399.9 and 599.9 MHz and ¹³C at 100.6 and 125.7 MHz at 25 °C. Chemical shifts (δ) are reported in ppm and coupling constants (J) are reported in hertz (Hz). Exact molecular masses were determined on Micromass Q-ToF2 mass spectrometer equipped with an electrospray ion source. Analytical RP-HPLC-MS was performed on a Gilson RP-HPLC system with a Finnigan AQA quadrupole low-resolution mass spectrometer in positive or negative ESI mode using a Onyx Monolithic C₁₈ 3 × 50 mm, 2.6 μm particle size, 100 Å pore size (Phenomenex) with gradients of MeCN in 0.05 % aqueous HCOOH as mobile phase at a flow rate of 2 mL/min. Preparative RP-HPLC was performed on a system equipped with a Nucleodur C18 HTec 5 μm column (150 × 21.2 mm) or a Phenomenex C8 5 μm column (150 × 21.2 mm), using a H₂O/CH₃CN gradient with 0.1 % TFA or 0.05 % HCOOH gradient, flow rate 15 mL/min, using UV detection at 220 nm and 254 nm. High resolution molecular masses (HRMS) were determined on a Waters acuity UPLC mass spectrometer with an ESI source, 7-T hybrid linear ion trap (LTQ), flow rate 0.25 mL/min (MeCN/H₂O 1:1). Compounds **1a-c** and **5a-c** were purchased and used without further purification. Reagent **3** was made outside of this work in-house, synthesis is described in the WO2022220725 patent [24]. Compounds **S1-3** are described and characterized in the WO2022220725 patent. Characterization data of compound **S4** is found in the supplementary data and was made in-house following the same synthetic protocol as described in this work.

4.7. General method for chloromethyl ethyl ether (EOM-Cl) protection

To a solution of sulfonamide (1 equiv) and DIPEA (2 equiv) in dry DCM or THF, chloromethoxyethane (1.5 equiv) was added at room temperature and the reaction mixture was left stirring overnight. The crude mixture was washed with brine and the product was extracted with organic solvent.

4.8. General method for amide-coupling using propylphosphonic anhydride (T3P)

To a solution of carboxylic acid **2a-2c** (1 equiv), aniline **3** (2-(4-((4-aminophenyl)sulfonyl)piperazin-1-yl)-6-methylpyrimidine-4-carbonitrile) (1 equiv), and DIPEA (3.5 equiv) in EtOAc under nitrogen, a solution of 50 % T3P in EtOAc (2 equiv) and two small crystals of DMAP was added to the reaction mixture that was stirred for 3–8 h at 55 °C. After completion of the reaction, the solution was diluted with EtOAc and washed successively with 0.1 M HCl (aq), saturated NaHCO₃ solution, water, brine, dried (Na₂SO₄), and evaporated. The residue was purified by the appropriate method to give the desired amide.

4.9. Synthesis of 3-(methylsulfonamido)benzoic acid (**2a**)

Step I. Into a solution of commercially available methyl 3-aminobenzoate **1a** (3.31 mmol, 500 mg) in dry DCM (50 mL) and Et₃N (8.27 mmol, 1.15 mL), methane-sulfonyl chloride (6.62 mmol, 512 μL) was added dropwise to the solution at room temperature and stirred for 3h, monitored by TLC. After completion, the reaction was quenched with cold water and extracted with EtOAc (3 × 50 mL). The organic layer was washed with water, brine, then dried over sodium sulfate and concentrated. The resulting crude product was purified by column chromatography on silica gel with 20 % EtOAc in iso-hexane as eluent. The product was obtained as a white solid (626 mg, 83 % yield). **Step II.** The

white solid was dissolved in 60 mL of THF/EtOH/H₂O (3:2:1) and hydrolyzed by adding LiOH (14.6 mmol, 350 mg) to the solution and left stirring for 4h. After acidification with HCl the product was obtained by extraction with dichloromethane, resulting in 515 mg, 88 % yield. LC/MS (ESI) *m/z*: [M – H][–] 214.0. ¹H NMR (400 MHz, DMSO-*d*₆) δ 13.05 (broad s, 1H), 9.96 (s, 1H), 7.81 (m, 1H), 7.68 (m, 1H), 7.47 (m, 1H), 7.45 (m, 1H), 3.01 (s, 3H).

4.10. Synthesis of 3-iodo-5-(methylsulfonamido)benzoic acid (**2b**)

Step I. Into a solution of methyl 3-amino-5-iodo-benzoate (3.61 mmol, 1.00g), and Et₃N (5.77 mmol, 805 μL) in DCM (50 mL) over ice bath, methanesulfonyl-chloride (4.33 mmol, 335 μL) was added dropwise over 30 min and the reaction mixture was stirred at room temperature for 16 h. Then 1 M HCl (aq, 40 mL) was added and the mixture was extracted with DCM (40 mL). Organic layer was extracted with water, dried over Na₂SO₄, and concentrated *in vacuo* to give methyl 3-iodo-5-(methanesulfonamido)-benzoate (1.2 g, 93.6 %), which was used in the next step without additional purification. **Step II.** The white solid (3.38 mmol, 1.2 g) was hydrolyzed with LiOH (405 mg, 16.9 mmol) dissolved in 50 mL of THF/EtOH/H₂O (3:2:1) and left stirring overnight at room temperature. The crude was then acidified with HCl and the mixture extracted with DCM (80 mL). Organic layer was extracted with water, washed with brine and dried over Na₂SO₄, and concentrated *in vacuo* to give **2b** (1.0 g, 89 %) as white powder. LC/MS (ESI) *m/z*: 341.1 [M+H]⁺. ¹H NMR (400 MHz, DMSO-*d*₆) δ 11.99 (s, 1H), 10.15 (s, 1H), 7.94 (t, *J* = 1.5 Hz, 1H), 7.81 (dd, *J* = 2.2, 1.4 Hz, 1H), 7.77 (dd, *J* = 2.1, 1.5 Hz, 1H), 3.85 (s, 3H). ¹³C NMR (101 MHz, DMSO-*d*₆) δ 165.0, 140.7, 132.82, 132.80, 131.9, 119.2, 95.7, 40.1.

Synthesis of 2-chloro-6-(methylsulfonamido)isonicotinic acid (2c**).** **Step I.** Into a solution of methyl 2,6-dichloropyridine-4-carboxylate (4.37 mmol, 900 mg), methanesulfonamide (8.74 mmol, 831 mg), K₃PO₄ (9.61 mmol, 2.04 g), Xantphos (0.271 mmol, 157 mg, 6 mol%) and Pd₂dba₃ (0.0874 mmol, 80 mg, 2 mmol%) were added to a dry, nitrogen flushed flask. Dioxane (16.5 mL) was added and the solution degassed with nitrogen and the reaction was heated to 120 °C for 50 min. The reaction mixture was cooled down and filtered through Celite and evaporated under vacuum. The crude was purified by column chromatography with 0–60 % gradient of EtOAc in iso-Hexane and the product fractions were collected and concentrated resulting in 450 mg of **2c-ester** (39 % yield). LC/MS (ESI) *m/z*: [M+H]⁺ 307.2. ¹H NMR (400 MHz, Acetonitrile-*d*₃) δ 8.54 (broad s, 1H), 7.55 (d, *J* = 1.0 Hz, 1H), 7.46 (d, *J* = 1.1 Hz, 1H), 3.91 (s, 3H), 3.26 (s, 3H). **Step II.** The methyl-ester (1.70 mmol, 450 mg) was hydrolyzed with LiOH (8.59 mmol, 204 mg) dissolved in 50 mL of THF/EtOH/H₂O (3:2:1) and left stirring for 3 h at 40 °C. After full hydrolysis of the ester, acidification was done with formic acid and the product was obtained by extraction with EtOAc, resulting in 420 mg of light beige solid **2c**, 98 % yield. LC/MS (ESI) *m/z*: [M+H]⁺ 251.5, 96 % pure by LC-MS and was used without further purification.

4.11. Synthesis of N-(4-((4-(4-cyano-6-methylpyrimidin-2-yl)piperazin-1-yl)sulfonyl)phenyl)-3-methyl-sulfonamido)benzamide (**4a**)

Following the general method for T3P coupling, (methanesulfonamido)benzoic acid **2a** (0.112 mmol, 24.0 mg), aniline **3** (0.112 mmol, 40.0 mg), and DIPEA (0.391 mmol, 68 μL) in EtOAc (2 mL), T3P (0.223 mmol, 0.13 mL) was reacted and monitored by TLC. After completion the reaction mixture was diluted with EtOAc (15 mL), washed successively with saturated NaHCO₃ solution, water, brine, dried (Na₂SO₄) and evaporated. The residue was purified by preparative biphenyl-RP-HPLC (40–90 % gradient of 0.05 % HCOOH in MeCN/H₂O) and the fractions containing the desired product collected and lyophilized resulting in 22.5 mg (36 % yield) as white powder, >95 % pure by LC-MS. ¹H NMR (400 MHz, DMSO-*d*₆) δ 10.68 (s, 1H), 10.00 (s, 1H), 8.03 (AA' of an AA'XX', 2H), 7.75 (XX' of an AA'XX', 2H), 7.72 (m, 1H),

7.68 (m, 1H), 7.51 (m, 1H), 7.44 (m, 1H), 7.09 (s, 1H), 3.86-3.83 (m, 4H), 3.04 (s, 3H), 2.98-2.95 (m, 4H), 2.33 (s, 3H). ^{13}C NMR (101 MHz, DMSO) δ 171.2, 166.4, 160.8, 144.0, 140.6, 139.4, 136.2, 129.9, 129.3, 129.2, 123.3, 123.2, 120.5, 119.5, 116.9, 113.4, 46.1, 43.0, 39.9, 24.5.

HRMS-ESI: $\text{C}_{24}\text{H}_{25}\text{N}_7\text{O}_5\text{S}_2^+ [\text{M} - \text{H}]^+$; calcd: 554.1277, found: 554.1280.

4.12. Synthesis of *N*-(4-((4-(4-cyano-6-methylpyrimidin-2-yl)piperazin-1-yl)sulfonyl)phenyl)-3-iodo-5-(methylsulfonamido)benzamide (**4b**)

Following the general method for T3P coupling, the benzoic acid **2b** (1.42 mmol, 485 mg) in EtOAc (75 mL), DIPEA (4.98 mmol, 867 μL), T3P (2.84 mmol, 1.69 mL) and aniline **3** (1.42 mmol, 510 mg) was reacted. After LC-MS analysis showed full conversion the reaction mixture was concentrated and mixed with sat. sodium bicarbonate solution and extracted into EtOAc (3 x 100 mL). The organic extract was washed with water and brine, dried over magnesium sulfate and concentrated to give crude **4b**. The product was purified by preparative C18-column chromatography with a 40–100 % gradient of 0.05 % formic acid in MeCN/H₂O for 30 min, resulting in 387 mg (40 % yield) of the product as white crystal. $\text{C}_{24}\text{H}_{24}\text{N}_7\text{O}_5\text{S}_2^+ [\text{M} + \text{H}]^+$; calcd: 682.0403, found: 682.0394. ^1H NMR (500 MHz, DMSO-*d*₆) δ 10.74 (s, 1H), 8.48 (s, 1H), 8.04 (AA' of an AA'XX', 2H), 7.69 (XX' of an AA'XX', 2H), 7.52 (m, 1H), 7.47 (m, 1H), 7.40 (m, 1H), 7.06 (s, 1H), 3.82 (m, 4H), 2.93 (m, 4H), 2.70 (s, 3H), 2.31 (s, 3H). ^{13}C NMR (126 MHz, DMSO-*d*₆) δ 171.2, 166.4, 166.0, 160.7, 150.6, 144.2, 140.6, 137.1, 130.6, 129.1, 129.0, 124.8, 120.4, 119.6, 116.9, 113.4, 95.4, 46.1, 43.0, 24.5.

4.13. Synthesis of 2-chloro-*N*-(4-((4-(4-cyano-6-methylpyrimidin-2-yl)piperazin-1-yl)sulfonyl)phenyl)-6-methylsulfonamido)iso-nicotinamide (**4c**)

Following the general method for T3P coupling, the carboxylic acid **2c** (0.123 mmol, 30.8 mg), aniline **3** (0.112 mmol, 40.0 mg), and DIPEA (0.391 mmol, 68 μL) in EtOAc (4 mL) was mixed with T3P (0.223 mmol, 0.24 mL). After conversion, the reaction mixture was diluted with EtOAc (15 mL), washed successively with saturated NaHCO₃ solution, water, brine, dried (Na₂SO₄) and evaporated. The residue was purified by preparative RP-HPLC (50–80 % gradient of 0.05 % HCOOH in MeCN/H₂O) and the fractions containing the desired product collected and lyophilized resulting in 51.0 mg (61 % yield) as white powder, >97 % pure by LC-MS. ^1H -NMR (400 MHz, DMSO-*d*₆) δ 11.26 (s, 1H), 11.02 (s, 1H), 8.03 (AA' of an AA'XX', 2H), 7.77 (XX' of an AA'XX', 2H), 7.66 (s, 1H), 7.35 (s, 1H), 7.09 (s, 1H), 3.91–3.78 (m, 4H), 3.01–, 2.91 (m, 4H), 2.33 (s, 3H), 2.09 (s, 3H). ^{13}C NMR (101 MHz, Acetone-*d*₆) δ 171.8, 161.9, 161.4, 153.9, 150.7, 143.7, 141.8, 131.7, 129.9, 121.1, 121.0, 117.2, 116.8, 113.6, 109.8, 46.8, 43.8, 42.1, 24.4. HRMS-ESI: $\text{C}_{23}\text{H}_{23}\text{ClN}_8\text{O}_5\text{S}_2^+ [\text{M} + \text{H}]^+$ calcd: 591.1000, found: 591.0995.

4.14. Synthesis of 3-(3-(aminomethyl)azetidin-1-yl)-*N*-(4-((4-(4-cyano-6-ethylpyrimidin-2-yl)piperazin-1-yl)sulfonyl)phenyl)-5-methylsulfonamido)-benzamide (**6a**)

Step I. Following the general method for EOM-protection of the sulfonamide, the Iodo-benzamide **4b** (0.0757 mmol, 51.6 mg), EOM-Cl (0.114 mmol, 10.5 μL) and DIPEA (0.151 mmol, 26.4 μL) was reacted. After full conversion was seen by LC-MS the crude product was washed with sat. NaHCO₃ solution, water, brine, and dried (Na₂SO₄) and evaporated. The EOM-protected intermediate was used further in next step without further purification. **Step II.** The EOM-protected intermediate (0.0338 mmol, 25.0 mg) was dissolved in toluene (7 mL) and commercially available *tert*-butyl *N*-(azetidin-3-ylmethyl)carbamate hydrochloride **5a** (0.0372 mmol, 8.28 mg) and potassium phosphate (0.0423 mmol, 8.97 mg) was added and flushed with nitrogen for 5 min. In a separate vial, Pd₂(dba)₃ (0.00270 mmol, 2.48 mg) and Xanthphos (0.0845 mmol, 4.89 mg) was dissolved in 1.0 mL toluene and flushed

with nitrogen then added to the reaction mixture, heated to 90 °C and stirred overnight. After conversion, the reaction mixture was diluted with EtOAc (20 mL), washed with saturated NaHCO₃ solution, water, brine, dried (Na₂SO₄) and evaporated. The residue was purified by preparative C18-HPLC with gradient 80–100 % of 20 mM triethyl ammonium acetate (TEAA) (MeCN/H₂O) and resulted in 20.4 mg of white solid (76 % yield). ^1H NMR (400 MHz, Chloroform-*d*) δ 8.50 (s, 1H), 8.02 (m, 1H), 7.87 (AA' of an AA'XX', 2H), 7.75 (XX' of an AA'XX', 2H), 7.53 (m, 1H), 7.41 (m, 1H), 6.64 (s, 1H), 5.00 (s, 2H), 3.96 (m, 4H), 3.90 (d, *J* = 9.4 Hz, 2H), 3.65 (m, 2H), 3.37 (m, 2H), 3.06 (m, 4H), 3.03 (s, 3H), 2.96 (m, 1H), 2.92 (m, 2H), 2.34 (s, 3H), 1.43 (m, 9H), 1.28 (t, *J* = 7.0 Hz, 3H). **Step III.** Into a solution of the protected intermediate from step II (0.0256 mmol, 20.4 mg) was dissolved in DCM (2 mL), and 1 mL of TFA was then added. The mixture was stirred for 3h at r.t. The crude mixture was concentrated to dryness and purified by preparative HPLC (C18 column, 30–35 % MeCN in water, 0.05 % formic acid buffer) and the fractions containing the desired product collected and lyophilized resulting in 11.0 mg (67 % yield) as white powder, >97 % pure by LC-MS. ^1H NMR (400 MHz, DMSO-*d*₆) δ 10.63 (s, 1H), 8.39 (s, 1H), 8.00 (AA' of an AA'XX', 2H), 7.72 (XX' of an AA'XX', 2H), 7.08 (s, 1H), 7.04 (s, 1H), 6.67 (m, 1H), 6.45 (m, 1H), 3.92 (m, 2H), 3.83 (m, 4H), 3.56 (m, 2H), 3.00 (s, 3H), 2.95 (m, 4H), 2.84 (m, 1H), 2.51 (m, 2H), 2.32 (s, 3H), 1.99 (m, 1H). ^{13}C NMR (126 MHz, DMSO-*d*₆) δ 171.2, 167.3, 166.9, 160.8, 152.7, 144.1, 140.6, 140.0, 136.8, 129.2, 129.5, 120.4, 116.9, 113.4, 108.0, 106.2, 105.2, 55.4, 46.1, 43.6, 43.0, 29.2, 24.5. HRMS-ESI: $\text{C}_{28}\text{H}_{33}\text{N}_9\text{O}_5\text{S}_2^+ [\text{M} + \text{H}]^+$ calcd: 640.2124, found: 640.2141.

4.15. Synthesis of 3-(azetidin-3-ylidenemethyl)-*N*-(4-((4-(4-cyano-6-methylpyrimidin-2-yl)piperazin-1-yl)sulfonyl)phenyl)-5-(methylsulfonamido)benzamide (**6b**)

Step I. To a solution of the Iodo-intermediate **4b** (0.0734 mmol, 50.0 mg), a commercially available Boc-protected boronic acid **5b** (0.147 mmol, 43.3 mg), 4 M aq. K₂CO₃ (0.293 mmol, 73.4 μL), Pd(PPh₃)₂ (0.00367 mmol, 4.24 mg) in 10 mL of toluene/EtOH (1:1) was added and reacted for 4 h at 85 °C. After conversion the crude mixture was washed with H₂O, brine and sat. K₂CO₃ (aq) and extracted with DCM followed by evaporation resulting in 32.0 mg light yellow crude product (60 % yield) that underwent purification after the next TFA deprotection step. **Step II.** The Boc-protected substrate from step I (32.0 mg, 0.0443 mmol) was dissolved in MeCN (3.5 mL), cooled to 0 °C and 3.5 mL of TFA was then added, then allowed to reach r.t. and stirred for 4h. The crude mixture was evaporated to dryness and purified by prep HPLC (C18 column, 30–60 % acetonitrile in water, 0.05 % formic acid buffer) and the fractions containing the desired product collected and lyophilized resulting in 17.0 mg (52 % yield) as white powder, >97 % pure by LC-MS. ^1H NMR (400 MHz, DMSO-*d*₆) δ 10.75 (s, 1H), 10.05 (s, 1H), 9.17 (s, 1H), 8.01 (AA' of an AA'XX', 2H), 7.75 (XX' of an AA'XX', 2H), 7.59 (s, 1H), 7.40 (s, 1H), 7.20 (m, 1H), 7.09 (s, 1H), 6.49 (s, 1H), 5.01 (m, 2H), 4.79 (m, 2H), 3.84 (m, 4H), 3.07 (s, 3H), 2.96 (m, 4H), 2.33 (s, 3H). ^{13}C NMR (126 MHz, DMSO-*d*₆) δ 170.8, 165.7, 160.3, 143.4, 140.1, 139.2, 136.5, 136.0, 131.2, 129.0, 128.7, 122.4, 121.7, 120.7, 120.0, 117.6, 116.4, 113.0, 56.0, 45.7, 45.6, 42.5, 40.1, 24.0. HRMS-ESI (*m/z*): $[\text{M} + \text{H}]^+$ calcd for $\text{C}_{28}\text{H}_{30}\text{N}_8\text{O}_5\text{S}_2$, 623.1853; found 623.1858.

4.16. Synthesis of 3-((3-(aminomethyl)azetidin-1-yl)methyl)-*N*-(4-((4-(4-cyano-6-methylpyrimidin-2-yl)piperazin-1-yl)sulfonyl)phenyl)-5-(methylsulfonamido)benzamide (**6c**)

Step I. Following the general method for EOM-protection of the sulfonamide, the Iodo-benzamide **4b** (0.293 mmol, 200 mg), EOM-Cl (0.440 mmol, 40.8 μL) and DIPEA (0.587 mmol, 102 μL) was reacted. After full conversion was seen by LC-MS the crude product was washed with sat. NaHCO₃ solution, water, brine, dried (Na₂SO₄) and evaporated resulting 200 mg of colourless product (97 % yield). The EOM-protected intermediate was used further in next step without further purification.

Step II. Triphenylphosphine (0.541 mmol, 142 mg) and iodine (0.541 mmol, 137 mg) were mixed in 40 mL toluene and stirred vigorously for 15 min. The EOM-protected iodo-intermediate from step I (0.270 mmol, 200 mg), palladium acetate (0.0389 mmol, 8.74 mg) and Et₃N (5.41 mmol, 754 μL) is then added. Formic acid (2.70 mmol, 106 μL) was slowly injected with a syringe into the reaction vessel via septum. The mixture is then stirred vigorously and heated at 80 °C for 3 h.

After cooling, the mixture is diluted with EtOAc and filtrated through a syringe filter, washed with water and brine. Purification by flash chromatography resulting in 100 mg white aldehyde intermediate (52 % yield). Half of the product was used in next step for the synthesis of **6c** (the other half was used further in the synthesis of **6d**). **Step III.** The aldehyde intermediate (0.0779 mmol, 50.0 mg) from step II was dissolved in 3 mL MeOH/THF (1:1) and reacted with the commercially available **5a** (0.156 mmol, 34.7 mg) and DIPEA (0.195 mmol, 33.9 μL) stirred overnight with magnesium sulfate (0.39 mmol, 46.9 mg). The next day the reaction mixture was cooled to 0 °C, and NaBH₄ (0.156 mmol, 5.90 mg) was added and the reaction mixture was allowed to reach r.t. and stirred for 1h. The crude mixture was then filtered and washed with water and brine and was used without further purification. **Step IV.** Finally, the Boc-protected substrate (0.0246 mmol, 20 mg) was dissolved in DCM (1.5 mL), cooled to 0 °C and 1.5 mL of TFA was then added. The mixture was stirred at r.t. for 2h. The mixture was then evaporated to dryness and purified by preparative HPLC (C18 column, 20–60 % acetonitrile in water, 0.05 % formic acid buffer) and the fractions containing the desired product collected and lyophilized resulting in 6.28 mg (39 % yield) as white powder, >95 % pure by LC-MS. ¹H NMR (400 MHz, Acetonitrile-*d*₃) δ 9.86 (s, 1H), 8.07 (AA' of an AA'XX', 2H), 7.89 (m, 2H), 7.74 (XX' of an AA'XX', 2H), 7.57 (s, 1H), 6.81 (s, 1H), 4.28 (s, 2H), 4.06 (d, *J* = 8.9 Hz, 2H), 3.93 (m, 2H), 3.88 (m, 4H), 3.26 (m, 2H), 3.20 (m, 1H), 3.05 (m, 4H), 3.02 (s, 3H), 2.33 (s, 3H). ¹³C NMR (101 MHz, Acetonitrile-*d*₃) δ 165.7, 161.6, 144.1, 141.3, 139.8, 133.4, 130.5, 129.3, 124.9, 124.9, 121.0, 120.7, 117.0, 113.4, 58.4, 56.7, 46.3, 43.5, 41.6, 39.7, 28.1, 24.1. HRMS-ESI: C₂₉H₃₆N₉O₅S₂⁺ [M+H]⁺ calcd: 654.2274, found: 654.2281.

4.17. Synthesis of 3-(((3-aminopropyl)amino)methyl)-N-(4-((4-cyano-6-methylpyrimidin-2-yl)piperazin-1-yl)sulfonyl)phenyl)-5-(methylsulfonamido)benzamide (**6d**)

The rest of the aldehyde intermediate product (0.0779 mmol, 50.0 mg) from step II in the synthesis of **6c** was dissolved in 3 mL MeOH/THF (1:1) and reacted with the commercially available **5c** (0.233 mmol, 40.7 mg) and stirred overnight at r.t. with magnesium sulfate (0.467 mmol, 56.3 mg). The next day the reaction mixture was cooled to 0 °C, and NaBH₄ (0.156 mmol, 5.90 mg) was added and the reaction mixture was allowed to reach r.t. and stirred for 1 h. The crude mixture was then filtered and washed with water and brine and was used without further purification.

Step II. The Boc-protected substrate (0.0375 mmol, 30.0 mg) was dissolved in DCM (2.5 mL), cooled to 0 °C and 2.5 mL of TFA was then added and stirred at r.t. for 3h. The crude mixture was evaporated to dryness a purified by preparative HPLC (C18 column, 30–60 % acetonitrile in water, 0.05 % formic acid buffer) and the fractions containing the desired product collected and lyophilized resulting in 15.1 mg (63 % yield) as pale yellow powder, >97 % pure by LC-MS. ¹H NMR (400 MHz, Acetonitrile-*d*₃) δ 8.16 (s, 1H), 7.99 (AA' of an AA'XX', 2H), 7.82 (m, 1H), 7.78 (m, 1H), 7.74 (XX' of an AA'XX', 2H), 7.56 (m, 1H), 6.82 (s, 1H), 4.17 (s, 2H), 3.86 (m, 4H), 3.10 (m, 2H), 3.04 (m, 2H), 3.02 (m, 4H), 3.01 (m, 2H), 2.55 (s, 3H), 2.31 (s, 3H), 2.06 (m, 2H). ¹³C NMR (101 MHz, Acetonitrile-*d*₃) δ 172.0, 166.8, 162.0, 144.2, 141.6, 139.9, 137.5, 134.6, 131.0, 129.8, 125.9, 121.4, 121.3, 117.4, 114.0, 51.7, 46.7, 45.5, 43.9, 40.7, 40.0, 37.8, 24.7, 24.5. HRMS-ESI: C₂₈H₃₅N₉O₅S₂⁺ [M+H]⁺ calcd: 642.2281, found: 642.2283.

4.18. Synthesis of 2-(3-(aminomethyl)azetidin-1-yl)-N-(4-((4-cyano-6-methylpyrimidin-2-yl)piperazin-1-yl)sulfonyl)phenyl)-6-(methylsulfonamido)isonicotinamide (**7**)

Step I. Following the general method for EOM-protection of the sulfonamide, the chloro-pyridine **4c** (0.0863 mmol, 51 mg), EOM-Cl (0.129 mmol, 12.0 μL) and DIPEA (0.173 mmol, 30.1 μL) was reacted in 6 mL dry THF. After full conversion was seen by LC-MS the crude product was washed with sat. NaHCO₃ solution, water, brine, dried (Na₂SO₄) and evaporated resulting 55.5 mg of pale-yellow solid (99 % yield). The EOM-protected intermediate was used further in next step without further purification. **Step II.**

The EOM-protected intermediate (0.0855 mmol, 55.5 mg) was dissolved in toluene (12 mL) and commercially available *tert*-butyl N-(azetidin-3-ylmethyl)carbamate hydrochloride **5a** (0.103 mmol, 22.8 mg) and cesium carbonate (0.256 mmol, 83.6 mg) was added and flushed with nitrogen for 5 min. In a separate vial, Pd₂(dba)₃ (0.00684 mmol, 6.26 mg) and RuPhos (0.0137 mmol, 6.38 mg) was dissolved in 3.0 mL toluene and flushed with nitrogen then added to the reaction mixture, heated to 90 °C and stirred overnight. After conversion, the reaction mixture was diluted with EtOAc (20 mL), washed with saturated NaHCO₃ solution, water, brine, dried (Na₂SO₄) and evaporated. The residue was purified on silica with EtOAc/iso-hexanes gradient 40–100 % EtOAc. The fractions with the product was collected and concentrated (39.5 mg, 58 % yield) and deprotected in next step. **Step III.** The Boc-protected substrate (0.0494 mmol, 39.5) was dissolved in DCM (2 mL), and 2 mL of TFA was then added. The mixture was stirred for 3 h at r.t. Evaporation to dryness a purified by preparative HPLC (C18 column, 30–90 % acetonitrile in water, 0.05 % formic acid buffer) and the fractions containing the desired product collected and lyophilized resulting in 28.0 mg (88 % yield) as white powder, >97 % pure by LC-MS. ¹H NMR (400 MHz, DMSO-*d*₆) δ 10.71 (m, 1H), 8.34 (m, 1H), 7.99 (AA' of an AA'XX', 2H), 7.73 (XX' of an AA'XX', 2H), 7.09 (s, 1H), 6.53 (m, 1H), 6.39 (m, 1H), 4.04 (m, 2H), 3.84 (m, 4H), 3.74 (m, 2H), 3.51 (m, 2H), 3.33 (s, 3H), 2.96 (m, 4H), 2.87 (m, 1H), 2.32 (s, 3H), 2.07 (m, 2H, NH₂). ¹³C NMR (126 MHz, DMSO-*d*₆) δ 171.2, 165.9, 160.8, 160.1, 153.3, 145.3, 143.7, 140.6, 129.2, 120.6, 116.9, 113.5, 98.5, 96.6, 60.1, 54.1, 46.1, 44.1, 43.0, 42.8, 30.6, 24.5. HRMS-ESI: C₂₇H₃₂N₁₀O₅S₂⁺ [M+H]⁺ calcd: 641.2077, found: 641.2067.

4.19. Synthesis of N-(4-((4-(3,5-dichlorophenyl)piperazin-1-yl)sulfonyl)phenyl)-3-(methylsulfonamido)benzamide (**S4**)

The 3-(methylsulfonamido)benzoic acid (0.311 mmol, 66.9 mg) was suspended in 3 mL DCM/DMF (1:1) and then oxalyl chloride (0.93 mmol, 70 μL) was added and the reaction mixture heated for 3 h at 50 °C. After conversion the solvent was removed under reduced pressure, affording the product which was dissolved in 1.5 mL DCM. This solution was added dropwise to solution of 4-[4-(3,5-dichlorophenyl)piperazin-1-yl]sulfonylaniline (0.311 mmol, 120 mg) in 1.5 mL pyridine. The reaction mixture was stirred at RT for 24 h, diluted with 15 mL of water and extracted with EtOAc (3 x 10 mL). The organic solution was washed with H₂O (3 x 10 mL), KH₂PO₄ (pH 4, 10 mL) and brine (10 mL), then dried over MgSO₄ and evaporated resulting in 175 mg crude product. The crude was purified on silica gel with 1–5% MeOH in DCM affording 50.0 mg white solid (28 % yield).

CRedit authorship contribution statement

Andrea Benediktsdottir: Writing – review & editing, Writing – original draft, Visualization, Project administration, Methodology, Investigation, Data curation. **Sanjeevani Sooriyaarachchi:** Investigation. **Sha Cao:** Investigation. **Nina E. Ottosson:** Investigation. **Stefan Lindström:** Investigation. **Bo Lundgren:** Investigation. **Katharina Kloditz:** Investigation. **Daina Lola:** Investigation. **Olga Bobileva:** Investigation. **Einars Loza:** Investigation. **Diarmaid Hughes:** Writing –

review & editing, Supervision, Resources, Funding acquisition. **T. Alwyn Jones:** Supervision, Investigation. **Sherry L. Mowbray:** Writing – review & editing, Supervision, Resources, Investigation. **Edouard Zamaratski:** Writing – review & editing, Supervision, Conceptualization. **Anja Sandström:** Writing – review & editing, Supervision. **Anders Karlén:** Writing – review & editing, Supervision, Resources, Funding acquisition.

Declaration of competing interest

The authors declare the following financial interests/personal relationships which may be considered as potential competing interests:

S.L., S.L.M., T.A.J, E.L., D.H., E.Z. and A.K. are authors on a patent application related to this work (publication no. WO 2022/220725, application no. PCT/SE2022/050360, filed on October 20, 2022). The authors declare no other competing interests.

Data availability

Data will be made available on request.

Acknowledgements

The authors acknowledge the support of ENABLE-2, a national platform for antibiotics development funded by the Swedish Research Council and the National research programme on antibiotic resistance (Dnr 2021–06603). A.K. acknowledges Swedish Research Council support (Dnr 2022-00654). D.H. acknowledges Swedish Research Council support (Dnr 2021–04814). We also acknowledge the support from the Chemical Biology Consortium Sweden (CBCS), the node in Linköping University. CBCS is a national research infrastructure funded by the Swedish Research Council (Dnr 2021-00179) and SciLifeLab. The graphical abstract was partly created using [Biorender.com](https://biorender.com).

Appendix A. Supplementary data

Supplementary data to this article can be found online at <https://doi.org/10.1016/j.ejmech.2024.116790>.

References

- [1] M.S. Butler, V. Gigante, H. Sati, S. Paulin, L. Al-Sulaiman, J.H. Rex, P. Fernandes, C.A. Arias, M. Paul, G.E. Thwaites, L. Czaplowski, R.A. Alm, C. Lienhardt, M. Spigelman, L.L. Silver, N. Ohmagari, R. Kozlov, S. Harbarth, P. Beyer, Analysis of the clinical pipeline of treatments for drug-resistant bacterial infections: despite progress, more action is needed, *Antimicrob. Agents Chemother.* 66 (2022), <https://doi.org/10.1128/aac.01991-21>.
- [2] T. Mestrovic, G. Robles Aguilar, L.R. Swetschinski, K.S. Ikuta, A.P. Gray, N. Davis Weaver, C. Han, E.E. Wool, A. Gershberg Hayoon, S.I. Hay, C. Dolecek, B. Sartorius, C.J.L. Murray, I.Y. Addo, B.O. Ahinkorah, A. Ahmed, M.A. Aldeyab, K. Allel, R. Anuceanu, A.E. Anyasodor, M. Ausloos, F. Barra, A.S. Bhagavathula, D. Bhandari, S. Bhaskar, N. Cruz-Martins, A. Dastiridou, K. Dokova, E. Dubljanin, O.C. Durojaiye, A.F. Fagbamigbe, S. Ferrero, P.A. Gaal, V.B. Gupta, V.K. Gupta, V. K. Gupta, C. Herteliu, S. Hussain, I.M. Ilic, M.D. Ilic, E. Jamshidi, T. Joo, A. Karch, A. Kisa, S. Kisa, T. Kostyanov, H.H. Kyu, J. Lám, G. Lopes, A.G. Mathioudakis, A.-F. A. Mentis, I.M. Michalek, M.A. Moni, C.E. Moore, F. Mulita, I. Negroi, R.I. Negroi, T. Palicz, A. Pana, J. Perdigão, I.-R. Petcu, N. Rabiee, D.L. Rawaf, S. Rawaf, M. Z. Shakhmardanov, A. Sheikh, L.M.L.R. Silva, V.Y. Skryabin, A.A. Skryabina, B. Socea, A. Stergachis, T.Z. Stoeva, C.D. Sumi, A. Thiyagarajan, M.R. Tovani-Palome, M. Yesiltepe, S. Bin Zaman, M. Naghavi, The burden of bacterial antimicrobial resistance in the WHO European region in 2019: a cross-country systematic analysis, *Lancet Public Health* 7 (2022) 897–913, [https://doi.org/10.1016/S2468-2667\(22\)00225-0](https://doi.org/10.1016/S2468-2667(22)00225-0).
- [3] C.J.L. Murray, K.S. Ikuta, F. Sharara, L. Swetschinski, G. Robles Aguilar, A. Gray, C. Han, C. Bisignano, P. Rao, E. Wool, S.C. Johnson, A.J. Browne, M.G. Chipeta, F. Fell, S. Hackett, G. Haines-Woodhouse, B.H. Kashef Hamadani, E.A.P. Kumaran, B. McManigal, S. Achalapong, R. Agarwal, S. Akech, S. Albertson, J. Amuasi, J. Andrews, A. Aravkin, E. Ashley, F.-X. Babin, F. Bailey, S. Baker, B. Basnyat, A. Bekker, R. Bender, J.A. Berkley, A. Bethou, J. Bielicki, S. Boonkasidecha, J. Bukosia, C. Carvalho, C. Castañeda-Orjuela, V. Chansamouth, S. Chaurasia, S. Chiurchiù, F. Chowdhury, R. Clotaire Donatien, A.J. Cook, B. Cooper, T. R. Cressey, E. Criollo-Mora, M. Cunningham, S. Darboe, N.P.J. Day, M. De Luca, K. Dokova, A. Dramowski, S.J. Dunachie, T. Duong Bich, T. Eckmanns, D. Eibach,

- A. Emami, N. Feasey, N. Fisher-Pearson, K. Forrest, C. Garcia, D. Garrett, P. Gastmeier, A.Z. Giref, R.C. Greer, V. Gupta, S. Haller, A. Haselbeck, S.I. Hay, M. Holm, S. Hopkins, Y. Hsia, K.C. Iregebu, J. Jacobs, D. Jarovsky, F. Javanmardi, A. W.J. Jenney, M. Khorana, S. Khusuwan, N. Kissoon, E. Kobeissi, T. Kostyanov, F. Krapp, R. Krumkamp, A. Kumar, H.H. Kyu, C. Lim, K. Lim, D. Limmathurotsakul, M.J. Loftus, M. Lunn, J. Ma, A. Manoharan, F. Marks, J. May, M. Mayxay, N. Mturi, T. Munera-Huertas, P. Musicha, L.A. Musila, M.M. Mussi-Pinhata, R.N. Naidu, T. Nakamura, R. Nanavati, S. Nangia, P. Newton, C. Ngoun, A. Novotney, D. Nwakanma, C.W. Obiero, T.J. Ochoa, A. Olivas-Martinez, P. Olliaro, E. Ooko, E. Ortiz-Brizuela, P. Ounchanum, G.D. Pak, J.L. Paredes, A.Y. Peleg, C. Perrone, T. Phe, K. Phommason, N. Plakkal, A. Ponce-de-Leon, M. Raad, T. Ramdin, S. Rattanavong, A. Riddell, T. Roberts, J.V. Robotham, A. Roca, V.D. Rosenthal, K. E. Rudd, N. Russell, H.S. Sader, W. Saengchan, J. Schnell, J.A.G. Scott, S. Seekaew, M. Sharland, M. Shivamallappa, J. Sifuentes-Osornio, A.J. Simpson, N. Steenkeste, A.J. Stewardson, T. Stoeva, N. Takak, A. Thaiprakong, G. Thwaites, C. Tigoi, C. Turner, P. Turner, H.R. van Doorn, S. Velaphi, A. Vongspradith, M. Vongsouvath, H. Vu, T. Walsh, J.L. Walson, S. Waner, T. Wangrangsimakul, P. Wannapinij, T. Wozniak, T.E.M.W. Young Sharma, K.C. Yu, P. Zheng, B. Sartorius, A.D. Lopez, A. Stergachis, C. Moore, C. Dolecek, M. Naghavi, Global burden of bacterial antimicrobial resistance in 2019: a systematic analysis, *Lancet* 399 (2022) 629–655, [https://doi.org/10.1016/S0140-6736\(21\)02724-0](https://doi.org/10.1016/S0140-6736(21)02724-0).
- [4] Geneva: World Health Organization, WHO Bacterial Priority Pathogens List, 2024: bacterial pathogens of public health importance to guide research, development and strategies to prevent and control antimicrobial resistance. <https://www.who.int/publications/i/item/9789240093461>, 2024.
- [5] Geneva: World Health Organization, 2023 antibacterial agents in clinical and preclinical development. <https://www.who.int/publications/i/item/9789240021303>, 2024.
- [6] N.K. Prasad, I.B. Seiple, R.T. Cirz, O.S. Rosenberg, Leaks in the pipeline: a failure analysis of gram-negative antibiotic development from 2010 to 2020, *Antimicrob. Agents Chemother.* 66 (2022), <https://doi.org/10.1128/aac.00054-22>.
- [7] K. Takayama, N. Qureshi, P. Mascagni, Complete structure of lipid A obtained from the lipopolysaccharides of the heptoseless mutant of *Salmonella typhimurium*, *J. Biol. Chem.* 258 (1983) 12801–12803, [https://doi.org/10.1016/s0021-9258\(17\)44040-3](https://doi.org/10.1016/s0021-9258(17)44040-3).
- [8] K. Takayama, N. Qureshi, P. Mascagni, M.A. Nashed, L. Anderson, C.R. Raetz, Fatty acyl derivatives of glucosamine 1-phosphate in *Escherichia coli* and their relation to lipid A. Complete structure of A diacyl GlcN-1-P found in a phosphatidylglycerol-deficient mutant, *J. Biol. Chem.* 258 (1983) 7379–7385, [https://doi.org/10.1016/s0021-9258\(18\)32190-2](https://doi.org/10.1016/s0021-9258(18)32190-2).
- [9] D.N. Crowell, M.S. Anderson, C.R.H. Raetz, Molecular cloning of the genes for lipid A disaccharide synthase and UDP-N-acetylglucosamine acyltransferase in *Escherichia coli*, *J. Bacteriol.* 168 (1986) 152–159, <https://doi.org/10.1128/jb.168.1.152-159.1986>.
- [10] M.S. Anderson, C.E. Bulawa, C.R.H. Raetz, The biosynthesis of gram-negative endotoxin. Formation of lipid A precursors from UDP-GlcNAc in extracts of *Escherichia coli*, *J. Biol. Chem.* 260 (1985) 15536–15541, [https://doi.org/10.1016/s0021-9258\(17\)36289-0](https://doi.org/10.1016/s0021-9258(17)36289-0).
- [11] C.R.H. Raetz, C.M. Reynolds, M.S. Trent, R.E. Bishop, Lipid A modification systems in gram-negative bacteria, *Annu. Rev. Biochem.* 76 (2007) 295–329, <https://doi.org/10.1146/annurev.biochem.76.010307.145803>.
- [12] C.R.H. Raetz, Z. Guan, B.O. Ingram, D.A. Six, F. Song, X. Wang, J. Zhao, Discovery of new biosynthetic pathways: the lipid A story, *J. Lipid Res.* 50 (2009) 103–108, <https://doi.org/10.1194/jlr.R800060-JLR200>.
- [13] C. Okada, H. Wakabayashi, M. Kobayashi, A. Shinoda, I. Tanaka, M. Yao, Crystal structures of the UDP-diacetylglucosamine pyrophosphohydrolase LpxH from *Pseudomonas aeruginosa*, *Sci. Rep.* 6 (2016) 1–9, <https://doi.org/10.1038/srep32822>.
- [14] H.E. Young, J. Zhao, J.R. Barker, Z. Guan, R.H. Valdivia, P. Zhou, Discovery of the elusive UDP-diacetylglucosamine hydrolase in the lipid A biosynthetic pathway in *Chlamydia trachomatis*, *mBio* 7 (2016) 1–10, <https://doi.org/10.1128/mBio.00090-16>.
- [15] L.E. Metzger, C.R.H. Raetz, An alternative route for UDP-diacetylglucosamine hydrolysis in bacterial lipid A biosynthesis, *Biochemistry* 49 (2010) 6715–6726, <https://doi.org/10.1021/bi1008744>.
- [16] D.L. Richie, K.T. Takeoka, J. Bojkovic, L.E. Metzger, C.M. Rath, W.S. Sawyer, J. R. Wei, C.R. Dean, Toxic accumulation of Ips pathway intermediates underlies the requirement of LpxH for growth of *Acinetobacter baumannii* ATCC 19606, *PLoS One* 11 (2016) 1–22, <https://doi.org/10.1371/journal.pone.0160918>.
- [17] P. Zhou, J. Hong, Structure- and ligand-dynamics-based design of novel antibiotics targeting lipid A enzymes LpxC and LpxH in gram-negative bacteria, *Acc. Chem. Res.* 54 (2021) 1623–1634, <https://doi.org/10.1021/acs.accounts.0c00880>.
- [18] J. Cho, C.-J. Lee, J. Zhao, H.E. Young, P. Zhou, Structure of the essential *Haemophilus influenzae* UDP-diacetylglucosamine pyrophosphohydrolase LpxH in lipid A biosynthesis, *Nat. Microbiol.* 1 (2016) 16154, <https://doi.org/10.1038/nmicrobiol.2016.154>.
- [19] A.S. Nayar, T.J. Dougherty, K.E. Ferguson, A.A. Granger, L.G. McWilliams, C. Stacey, L.J. Leach, S. ichiro Narita, H. Tokuda, B.A. Miller, D.G. Brown, S.M. McLeod, Novel antibacterial targets and compounds revealed by a high-throughput cell wall reporter assay, *J. Bacteriol.* 197 (2015) 1726–1734, <https://doi.org/10.1128/JB.02552-14>.
- [20] S.-H. Kwak, C.S. Cochrane, A.F. Ennis, W.Y. Lim, C.G. Webster, J. Cho, B.A. Fenton, P. Zhou, J. Hong, Synthesis and evaluation of sulfonyl piperazine LpxH inhibitors, *Bioorg. Chem.* 102 (2020) 104055, <https://doi.org/10.1016/j.bioorg.2020.104055>.

- [21] M. Lee, J. Zhao, S.H. Kwak, J. Cho, M. Lee, R.A. Gillespie, D.Y. Kwon, H. Lee, H. J. Park, Q. Wu, P. Zhou, J. Hong, Structure-activity relationship of sulfonyl piperazine LpxH inhibitors analyzed by an LpxE-coupled malachite green assay, *ACS Infect. Dis.* 5 (2019) 641–651, <https://doi.org/10.1021/acinfecdis.8b00364>.
- [22] J. Cho, M. Lee, C.S. Cochrane, C.G. Webster, B.A. Fenton, J. Zhao, J. Hong, P. Zhou, Structural basis of the UDP-diacetylglucosamine pyrophosphohydrolase LpxH inhibition by sulfonyl piperazine antibiotics, *Proc. Natl. Acad. Sci. USA* 117 (2020) 4109–4116, <https://doi.org/10.1073/pnas.1912876117>.
- [23] S. Kwak, C. Skyler Cochrane, J. Cho, P.A. Dome, A.F. Ennis, J.H. Kim, P. Zhou, J. Hong, Development of LpxH inhibitors chelating the active site dimanganese metal cluster of LpxH, *ChemMedChem* 18 (2023), <https://doi.org/10.1002/cmdc.202300023>.
- [24] E. Zamaratski, D. Antonov, V.R. Konda, S. Lindström, G. Olanders, A. Karlén, T. A. Jones, S.L. Mowbray, D. Hughes, P. Brandt, E. Loza, O. Bobileva, M. Ikaunieks, LpxH inhibitors as anti-infective agents, WO2022220725, https://patentscope.wipo.int/search/en/detail.jsf?docid=WO2022220725&_cid=P21-LO48G-8-03598-1, 2022.
- [25] D.L. Huseby, S. Cao, E. Zamaratski, S. Sooriyaarachchi, S. Ahmad, T. Bergfors, L. Krasnova, J. Pells, M. Ikaunieks, E. Loza, M. Katkevics, O. Bobileva, H. Cirule, B. Gukalova, S. Grinberga, M. Backlund, I. Simoff, A.T. Leber, T. Berruga-Fernández, D. Antonov, V.R. Konda, S. Lindström, G. Olanders, P. Brandt, P. Baranczewski, C. Vingsbo Lundberg, E. Liepinsh, E. Suna, T.A. Jones, S. L. Mowbray, D. Hughes, A. Karlén, Antibiotic class with potent in vivo activity targeting lipopolysaccharide synthesis in Gram-negative bacteria, *Proc. Natl. Acad. Sci. USA* 121 (2024) 1–8, <https://doi.org/10.1073/pnas.2317274121>.
- [26] K. Amrein, F. Dey, X. Ding, X. Huang, C. Lerner, H. Shi, X. Tan, J. Wu, J. Zheng, M. Zhou, Sulfonylpiperazinyl compounds for treatment of bacterial infections, WO2023061617, https://patentscope.wipo.int/search/en/detail.jsf?docid=WO2023061617&_cid=P21-LO486F-99976-1, 2023.
- [27] L. Provins, E. Jnoff, C. Genicot, Back-up strategies in drug discovery: what, how and when? *Drug Discov. Today* 19 (2014) 1808–1811, <https://doi.org/10.1016/j.drudis.2014.07.001>.
- [28] S.S. El Zahed, S. French, M.A. Farha, G. Kumar, E.D. Brown, Physicochemical and structural parameters contributing to the antibacterial activity and efflux susceptibility of small-molecule inhibitors of *Escherichia coli*, *Antimicrob. Agents Chemother.* 65 (2021), <https://doi.org/10.1128/AAC.01925-20>.
- [29] D. Gurvic, U. Zachariae, Multidrug efflux in Gram-negative bacteria: structural modifications in active compounds leading to efflux pump avoidance, *Npj Antimicrob. Resist.* 2 (2024) 1–11, <https://doi.org/10.1038/s44259-024-00023-w>.
- [30] M. Duffey, R.P. Jumde, R.M.A. da Costa, H.K. Ropponen, B. Blasco, L.J.V. Pidcock, Extending the potency and lifespan of antibiotics: inhibitors of gram-negative bacterial efflux pumps, *ACS Infect. Dis.* 10 (2024) 1458–1482, <https://doi.org/10.1021/acinfecdis.4c00091>.
- [31] Y. Wang, R. Alenzy, D. Song, X. Liu, Y. Teng, R. Mowla, Y. Ma, S.W. Polyak, H. Venter, S. Ma, Structural optimization of natural product nordihydroguareic acid to discover novel analogues as AcrB inhibitors, *Eur. J. Med. Chem.* 186 (2020) 111910, <https://doi.org/10.1016/j.ejmech.2019.111910>.
- [32] M.F. Richter, B.S. Drown, A.P. Riley, A. Garcia, T. Shirai, R.L. Svec, P. J. Hergenrother, Predictive compound accumulation rules yield a broad-spectrum antibiotic, *Nature* 545 (2017) 299–304, <https://doi.org/10.1038/nature22308>.
- [33] B.H. Asghar, Kinetic study of nucleophilic reactivity of heterocyclic amines with 4,6-dinitrobenzofuroxan in acetonitrile, *Arab. J. Chem.* 12 (2019) 2476–2483, <https://doi.org/10.1016/j.arabjc.2015.04.006>.
- [34] J.W. Warmke, B. Ganetzky, A family of potassium channel genes related to eag in *Drosophila* and mammals, *Proc. Natl. Acad. Sci. U.S.A.* 91 (1994) 3438–3442, <https://doi.org/10.1073/pnas.91.8.3438>.
- [35] C. Antzelevitch, S. Sicouri, Clinical relevance of cardiac arrhythmias generated by afterdepolarizations. Role of M cells in the generation of U waves, triggered activity and torsade de pointes, *J. Am. Coll. Cardiol.* 23 (1994) 259–277, [https://doi.org/10.1016/0735-1097\(94\)90529-0](https://doi.org/10.1016/0735-1097(94)90529-0).
- [36] Y. Kawai, S. Tsukamoto, J. Ito, K. Akimoto, M. Takahashi, A risk assessment of human ether-a-go-go-related gene potassium channel inhibition by using lipophilicity and basicity for drug discovery, *Chem. Pharm. Bull.* 59 (2011) 1110–1116, <https://doi.org/10.1248/cpb.59.1110>.
- [37] A. Garrido, A. Lepailleur, S.M. Mignani, P. Dallemagne, C. Rochais, hERG toxicity assessment: useful guidelines for drug design, *Eur. J. Med. Chem.* 195 (2020) 112290, <https://doi.org/10.1016/j.ejmech.2020.112290>.
- [38] M. De Rosa, L. Lu, E. Zamaratski, N. Szalaj, S. Cao, H. Wadensten, L. Lenhammar, J. Gising, A.K. Roos, D.L. Huseby, R. Larsson, P.E. Andrén, D. Hughes, P. Brandt, S. L. Mowbray, A. Karlén, Design, synthesis and in vitro biological evaluation of oligopeptides targeting *E. coli* type I signal peptidase (LepB), *Bioorg. Med. Chem.* 25 (2017) 897–911, <https://doi.org/10.1016/J.BMC.2016.12.003>.
- [39] E. Lindhagen, P. Nygren, R. Larsson, The fluorometric microculture cytotoxicity assay, *Nat. Protoc.* 3 (2008) 1364–1369, <https://doi.org/10.1038/nprot.2008.114>.
- [40] W. Kabsch, Research papers XDS research papers, *Acta Crystallogr. Sect. D Biol. Crystallogr.* 66 (2010) 125–132, <https://doi.org/10.1107/S0907444909047337>.
- [41] P.R. Evans, G.N. Murshudov, How good are my data and what is the resolution? *Acta Crystallogr. Sect. D Biol. Crystallogr.* 69 (2013) 1204–1214, <https://doi.org/10.1107/S0907444913000061>.
- [42] G.N. Murshudov, P. Skubák, A.A. Lebedev, N.S. Pannu, R.A. Steiner, R.A. Nicholls, M.D. Winn, F. Long, A.A. Vagin, REFMAC5 for the refinement of macromolecular crystal structures, *Acta Crystallogr. Sect. D Biol. Crystallogr.* 67 (2011) 355–367, <https://doi.org/10.1107/S0907444911001314>.
- [43] T.A. Jones, J.Y. Zou, S.W. Cowan, M. Kjeldgaard, Improved methods for building protein models in electron density maps and the location of errors in these models, *Acta Crystallogr., Sect. A* 47 (1991) 110–119, <https://doi.org/10.1107/S0108767390010224>.